Title

Full title: The archetypal gene transfer agent (RcGTA) is regulated via direct interaction with the enigmatic RNA polymerase omega subunit

Short Title: *Regulation of RcGTA production by GafA and Rpo-ω*

Authors

David Sherlock,[1] Paul C. M. Fogg[1,2]*

Affiliations

[1] Biology Department, University of York, York, United Kingdom. YO10 5DD

[2] York Biomedical Research Institute (YBRI), University of York, York, United Kingdom. YO10 5NG

* Corresponding author and lead contact: Dr Paul C.M. Fogg at paul.fogg@york.ac.uk

Summary

Gene transfer agents (GTAs) are small virus-like particles that indiscriminately package and transfer any DNA present in their host cell, with clear implications for bacterial evolution. The first transcriptional regulator that directly controls GTA expression, GafA, was recently discovered but its mechanism of action remained elusive. Here we demonstrate that GafA controls GTA gene expression by direct interaction with the RNA polymerase omega subunit (Rpo-ω) and also positively autoregulates its own expression by an Rpo-ω independent mechanism. We show that GafA is a modular protein with distinct DNA and protein binding domains. The functional domains we observe in Rhodobacter GafA also correspond to two-gene operons in Hyphomicrobiales pathogens. Together these data allow us to produce the most complete regulatory model for a GTA, and point towards an atypical mechanism for RNA polymerase recruitment and specific transcriptional activation in the alpha-proteobacteria.

INTRODUCTION

Horizontal gene transfer by viruses and other mobile genetic elements is the major driver of rapid bacterial adaptation and spread of traits such as antibiotic resistance. Gene Transfer Agents (GTAs) are virus-like genetic elements that are similar to viruses but instead of prioritizing the spread of their own genes, they package and disseminate any DNA within the host cell (Hynes *et al.*, 2016; Lang *et al.*, 2012; Shakya *et al.*, 2017; Sherlock *et al.*, 2019; Tamarit *et al.*, 2018). Although GTAs usually package and transfer 'random' fragments of DNA from their host to compatible recipients in headful fragments (Berglund *et al.*, 2009; Esterman *et al.*, 2021; Freese *et al.*, 2017; Hynes *et al.*, 2012; Sherlock *et al.*, 2019), some species do exhibit bias towards certain regions of the genome (Berglund *et al.*, 2009; Tomasch *et al.*, 2018). Significantly, GTAs have been implicated in high frequency spread of genes between bacteria (McDaniel *et al.*, 2010) and an extensive survey of the function of thousands of bacterial genes indicated that GTA genes convey significant fitness benefits in multiple species under stress conditions (Kogay *et al.*, 2019, 2020; Price *et al.*, 2018).

The true prevalence of GTAs is not currently known, however, a recent study identified homologues of the model *Rhodobacter capsulatus* GTA (RcGTA) is present in at least 50% of sequenced alpha-proteobacteria genomes – many of which had been mis-annotated as remnant prophages (Kogay *et al.*, 2019, 2020; Shakya *et al.*, 2017). The GTA genes are often dispersed at multiple genomic locations (Hynes *et al.*, 2016; Motro *et al.*, 2009), and co-ordinated expression initiates from a small subset of the bacterial population (Fogg, 2019; Fogg *et al.*, 2012; Hynes *et al.*, 2012; Québatte and Dehio, 2019). Timing and regulation of GTA production is tightly controlled by interlinked host regulatory circuits including quorum sensing (Koppenhöfer *et al.*, 2019; Leung *et al.*, 2012), stringent response (Québatte *et al.*, 2017; Westbye *et al.*, 2017), SOS response (Kuchinski *et al.*, 2016), c-di-GMP (Pallegar *et al.*, 2020b, 2020a) and the pleiotropic transcription factor CtrA (Lang and Beatty, 2000; Westbye *et al.*, 2018). In *R. capsulatus*, these complex pathways are integrated via a specific GTA transcriptional regulator, GafA (Fogg, 2019), and an RTX-domain extracellular repressor, *rcc00280* (Ding *et al.*, 2019; Westbye *et al.*, 2018). However, the precise mechanism of action for these proteins is not fully known.

It has been suggested that *Bartonella* GTAs are produced by the fittest cells in a given population in response to cytosolic ppGpp levels (Québatte *et al.*, 2017), and that RcGTA production is also influenced by ppGpp via the RNA polymerase omega sub-unit (Rpo-ω) (Westbye *et al.*, 2017). *R. capsulatus* Rpo-ω is not required for growth but is essential for RcGTA production (Westbye *et al.*, 2017). In other species, Rpo-ω is thought to play several roles including stabilization of the RNAP holoenzyme and modulation of transcription profiles via recruitment of alternative sigma factors (Gunnelius *et al.*, 2014; Paget, 2015; Ross *et al.*, 2013; Weiss *et al.*, 2017). One study showed that *E. coli* Rpo-ω can facilitate transcriptional activation when covalently linked to DNA binding proteins

(Dove and Hochschild, 1998), but to our knowledge no native interaction between Rpo-ω and a transcriptional regulator has ever been demonstrated. Here, we examine the relationship between RNAP-ω and the RcGTA activator protein, GafA. We explore the protein:protein and protein:DNA binding activities of GafA domains, identify putative *gafA* genes in pathogenic Hyphomicrobiales species and speculate on the overall mechanism of action for the GafA regulator.

RESULTS

Rpo-ω is required for activation of GTA production by GafA

GafA is the only known direct activator of Gene Transfer Agent expression in *R. capsulatus* (Fogg, 2019). The omega sub-unit of RNA polymerase (Rpo-ω), encoded by the *rpoZ* gene, is also required for RcGTA production (Westbye *et al.*, 2017) but the relationship between the two has not been established. Introduction of the plasmid pCMF180, containing *gafA* together with its native promoter, into wild-type *R. capsulatus* SB1003 leads to an increase in RcGTA production - presumably due to increased copy number (Fig. 1A & B); meanwhile deletion of *rpoZ* completely eliminates GTA production (Fig. 1A & B), both of which corroborate previous findings (Fogg, 2019; Westbye *et al.*, 2017). The pCMF180 plasmid was introduced into SB1003 Δ*rpoZ* to test whether moderate *gafA* overexpression can overcome the loss of RcGTA production phenotype but no GTA gene transfer was detected (Fig. 1B). Western blots of concentrated supernatants using an α-RcGTA capsid antibody also failed to detect any capsid protein accumulation in the supernatant of the SB1003 Δ*rpoZ* + *gafA* strains (Fig. 1A). As *gafA* was expressed from its own promoter, it is possible that Rpo-ω acts to regulate expression of *gafA* and consequently the GTA genes indirectly. To confirm that expression of *gafA* was not affected in any way by the loss of *rpoZ*, RNA was extracted for transcript quantification by qPCR. The transcription of *gafA* in SB1003 Δ*rpoZ* was equivalent to wild-type, and *gafA* transcript abundance was actually higher for SB1003 Δ*rpoZ* + pCMF180 compared to the *rpoZ* replete background (Fig. 1C). Finally, a construct was created containing *gafA* expressed from a non-native cumate inducible promoter – pCMF254. Overexpression of *gafA* in SB1003 led to an ~20-fold increase in GTA production, however, overexpression in SB1003 Δ*rpoZ* produced no detectable GTA production and was thus indistinguishable from the empty plasmid control (Fig. 1D). Taken together, these data indicate that Rpo-ω is not required for expression of *gafA* but instead regulates RcGTA production downstream.

Rpo-ω directly interacts with GafA

In multiple species Rpo-ω is thought to influence RNAP sigma factor preference and consequently global gene expression (Gunnelius *et al.*, 2014; Kurkela *et al.*, 2021; Mathew and Chatterji, 2006; Yamamoto *et al.*, 2018). We hypothesized that GafA acts by

binding to Rpo-ω to alter promoter preferences of the RNAP holoenzyme, and hence deletion of *rpoZ* abolishes the influence of GafA. pUT18 bacterial-2-hybrid plasmids were created with each of the *R. capsulatus* RNAP sub-units – α, β, β' and -ω, and tested for binding to T25-GafA. In this assay, a successful interaction between two proteins brings together the T18 and T25 domains of adenylate cyclase and ultimately leads to production of β-galactosidase, which can be measured using colorimetric substrates such as X-gal or O-nitrophenol (Karimova *et al.*, 1998). The α, β and β' sub-units all gave no detectable signal for interaction with GafA, while Rpo-ω produced a strong positive signal in a β-galactosidase assay (Fig. 2A). To confirm this result, MBP-GafA (Fogg, 2019) was bound to amylose magnetic beads and used as bait for capture of purified H6-Rpo-ω. Mock bait beads were simultaneously prepared by identical treatment but with GafA protein omitted. Addition of the Rpo-ω protein to mock beads produced no detectable binding, whereas Rpo-ω was detected in the eluate from the GafA pre-bound beads (Fig. 2B). These data confirm that GafA directly interacts with Rpo-ω, which is then likely to lead to changes in RNAP promoter selection and specific expression of RcGTA genes.

GafA homologues are present throughout the Rhodobacterales and Hyphomicrobiales

The GafA protein shares little primary sequence similarity with any well characterized proteins, but does possess localized similarity with DnaA and sigma factor DNA-binding domains at the N and C-terminal regions of the protein (Fogg, 2019). We performed a BLASTp sequence similarity search using the *R. capsulatus* GafA protein as a query, which revealed hits to genes annotated as DUF6456 domain or helix-turn-helix domain-containing proteins from widespread Rhodobacterales species (Table S1A). This agrees with a previous finding by that GafA homologues were present in all twenty-one complete Rhodobacterales genomes that were available at that time (Hynes *et al.*, 2016). A recent study by Kogay *et al.* (2019) proposed that 60% of the 730 available Hyphomicrobiales (formerly Rhizobiales) genome sequences contained putative RcGTA genes, however, this study only focused on genes within the core structural gene cluster and so did not include *gafA*. We performed additional PSI-BLAST and BLASTp sequence similarity searches with an *R. capsulatus* GafA protein query, but limited the results to the Hyphomicrobiales. Matches were produced to a wide variety species, though sequence similarity was localized to the C-terminal portion of the protein (Fig. S1, Table S1B & C), with the closest sequence similarity found in the final ~18 kDa. Notably, the majority of Hyphomicrobiales homologues were ~22-32 kDa, compared to the 42 kDa *R. capsulatus* GafA, but in most cases the "*gafA"* gene was preceded by a small gene predicted to encode a DnaA-like DNA-binding protein (Fig. S2). Local synteny was also conserved in the Hyphomicrobiales genomes with a downstream gene predicted to encode a cysteine desulfuration enzyme (*sufE*) and an upstream transcriptional regulator annotated as *mucR* or as an HTH-containing gene (Fig. S2). Occasional exceptions appear to be either

full length Rhodobacterales-type *gafA* genes with associated Rhodobacterales synteny or Hyphomicrobiales synteny but without a DnaA-like gene (Fig. S2C, Table S1D). Further BLASTp searches with taxonomic limits set for more distantly related Hyphomicrobiales pathogen species (Agrobacteria and Brucellaceae) produced similar results in terms of local synteny and sequence identity (Table S1E & F), suggesting that these genes and gene organization are common throughout the Order.

The GafA central region is important for protein:protein interactions

Meanwhile, we predicted the GafA structure from the primary protein sequence using the AlphaFold program (Jumper *et al.*, 2021). All five AlphaFold models placed the two putative DNA-binding domains in equivalent positions and orientations, linked by a central domain of unknown function (Fig. 3A&B). Informed by the structural model and the alignments to Hyphomicrobiales genes (Fig. S1), three bacterial-2-hybrid constructs were produced using truncated *gafA* gene fragments that encode residues 1-226 (N^{1-226}), 87-382 (Cx^{87-382}) and 221-382 ($C^{221-382}$) (Fig. 3A). The three constructs were tested for an interaction with Rpo-ω and both GafA-N^{1-226} and GafA-Cx^{87-382} produced a positive signal, but GafA-$C^{221-382}$ did not (Fig. 3C). To confirm this result, purified MBP-GafA-Cx^{87-382} protein was bound to amylose magnetic beads and used as bait for capture of H6-Rpo-ω in solution. Binding of Rpo-ω to the immobilized MBP-GafA-Cx^{87-382} protein was successfully detected (Fig. 3D). The GafA-N^{1-226} and GafA-Cx^{87-382} constructs overlap in central region of the protein, which suggests that this is the location of GafA:Rpo-ω binding. Additional bacterial-2-hybrid constructs were made to isolate the central region of GafA i.e. amino acids 87-212 (Cen2) and 87-226 (CenN). Both were positive for binding with Rpo-ω (Fig. 3C). These data indicate that GafA is comprised of two distal DNA binding domains and a central protein binding domain. The AlphaFold model (Fig. 3B & Fig. S3) predicted that the central region contains a beta-sheet motif (~amino acids 129-181) that is presented in the opposite direction to the DNA binding motifs, and we hypothesize that this is the interaction interface for Rpo-ω.

No experimental structures are available for Rpo-ω proteins from species that are closely related to *R. capsulatus.* An HHPRED search, using *R. capsulatus* Rpo-ω as a query, identified structural similarity matches across the first ~70 amino acids of the protein (Table S2A). AlphaFold models of *R. capsulatus* Rpo-ω closely matched *E. coli* Rpo-ω, but also lacked sufficient confidence at the C-terminal (Fig. S4A-C). The AlphaFold models of Rpo-$ω^{1-71}$ and GafA-CenN were submitted to the LZerD Web Server for protein docking prediction (Christoffer *et al.*, 2021). The results were not conclusive (highest rank sum score = 57) but 6 of the top 10 models predicted that binding occurs with the beta-sheet (Fig. S3D). Further experimental confirmation will be required to definitively pinpoint the binding interface.

GafA NT is not required for autoregulation but essential for GTA activation

To test whether different domains of GafA play different regulatory roles, three regions identified in Fig. 3 (GafA-N^{1-226}, $C^{221-382}$ and Cx^{87-382}) were cloned into the cumate inducible expression vector pQF. The pQF vectors were introduced into SB1003 wild-type and SB1003 Δ*gafA* strains and tested for various RcGTA production phenotypes. In a RcGTA gene transfer bioassay, GafA-N^{1-226} and GafA-$C^{221-382}$ were unable to induce any RcGTA production in either genetic background (Fig. 4A & S5A). Interestingly, overexpression of both GafA-Cx^{87-382} and full length GafA in wild-type cells stimulated ~80-100-fold greater gene transfer frequencies than the vector only control (Fig. 4A), however, neither were able to complement the *gafA* knock-out (Fig. S5A). These data were corroborated by visualization of intracellular ~4kb RcGTA DNA accumulation by gel electrophoresis (Fig. S5B), detection of characteristic bacteriochlorophyll absorbance peaks in cell-free supernatant indicative of cell lysis (Fig. S5C & D), and western blots to assess accumulation of the RcGTA capsid in the supernatant (Fig. S5E). In all cases, full length GafA and GafA-Cx^{87-382} induced RcGTA production and lysis in wild-type cells but no RcGTA production was detected for Δ*gafA* strains complemented with any *gafA* overexpression constructs. The GafA DnaA-like helix-turn-helix DNA binding motif is very close the N-terminus of the protein (~aa15-55, Fig. 3) and so it is possible that extra residues at this end of the protein interfere with DNA binding (Fogg, 2019). Previous work showed that the full length *gafA* ORF overexpressed from the *puf* photosynthesis promoter effectively complemented the Δ*gafA* mutant (Fogg, 2019), therefore, we produced comparable *puf*-GafA-Nc^{1-86} and N^{1-226} constructs and introduced them into SB1003 wild-type and SB1003 Δ*gafA* strains. Gene transfer bioassays showed that neither GafA-Nc^{1-86} nor N^{1-226} could complement the *gafA* knock-out and neither could induce RcGTA overexpression in the SB1003 wild-type (Fig. 4B & C). Meanwhile, *in trans* expression of full length GafA from the *puf* promoter complemented the SB1003 Δ*gafA* strain and increased SB1003 wild-type gene transfer frequencies by 43.5-fold, compared to the SB1003 plus empty vector control (Fig 4B & C).

The above data indicate that the presence of a short N-terminal Flag tag in the pQF vector impaired complementation, and that full-length GafA is required to induce RcGTA production. However, the fact that overexpression of a truncated *gafA* completely lacking the N-terminal DNA binding motif still induces high level RcGTA production in the presence of a full-length chromosomal copy of *gafA,* indicates that the GafA-Cx^{87-382} region (Fig. 3) can perform at least some of the functions of the full-length protein. We hypothesized that the GafA-Cx^{87-382} portion of the protein can activate the *gafA* promoter independent of the N-terminal DNA binding domain but the full protein is required for wider transcriptional activation of other RcGTA genes. To differentiate the effect of full length GafA and GafA-Cx^{87-382} on RcGTA gene expression in SB1003 wild-type and SB1003 Δ*gafA* cells, transcript abundance of the RcGTA capsid, endolysin and *gafA* genes were

measured by qPCR (Fig. 4D). We used *gafA* primers that bind within the region encoding GafA-Cx and, therefore, the qPCR measured the total combined transcripts of chromosomal and plasmid-borne *gafA* or *gafA*-Cx genes. As expected, overexpression of *gafA* or *gafA*-Cx$^{87-382}$ in either the wild-type or knock-out strain produced similar levels of *gafA* transcripts and, consistent with the phenotypic data, this only led to increased RcGTA capsid and endolysin production in wild-type cells. To quantify the activity of the chromosomal *gafA* promoter, we used primers designed to amplify the 5'-UTR that is present only on the chromosome and is also retained in the Δ*gafA* mutant. Transcription from the native promoter was upregulated more than 10-fold when *gafA* or *gafA*-Cx$^{87-382}$ were overexpressed in either wild-type or Δ*gafA* cells (Fig. 4D).

Mutation of key residues near the GafA N-terminus impairs RcGTA activation

In agreement with previous work (Fogg, 2019), an HHPRED search for structural homologues of GafA identified tentative hits against numerous sigma factors for both the predicted N- and C-terminal GafA DNA-binding domains (Table S2B-D); C-terminal DBD: E-value>0.84, N-terminal DBD: E-value ≥ 0.0017). However, the N-terminal DBD also produced hits against three DnaA proteins from diverse species in the PDB database, two of which produced E-values ≥ 8.5E-07, as well the DnaA entry from the NCBI conserved domain database (Table S2C). Alignment of the *R. capsulatus* GafA N-terminal region with *E. coli*, *Mycobacterium tuberculosis* and *Aquifex aeolicus* DnaA proteins showed poor primary sequence conservation overall but patches of increased sequence similarity particularly around the residues predicted to bind in the major groove of DNA (Fig. 5A) (Blaesing *et al.*, 2000; Fujikawa *et al.*, 2003).

Ten amino acid locations in the GafA protein were chosen based on sequence conservation or predicted involvement in DNA-binding (Fig. 5A-C). Each position was changed to alanine in the *gafA* complementation plasmid, pCMF180, by site directed mutagenesis. The mutated plasmids were introduced into SB1003 Δ*gafA* to assess the relative ability of each to restore RcGTA production. All mutations had a strong impact on protein function with average gene transfer frequencies at approximately 20% or less compared to the unmutated version of *gafA* (Fig. 5D). The plasmids were also introduced into a *gafA*-null derivative of the RcGTA overproducer strain, *R. capsulatus* DE442. The *gafA* gene is known to be expressed at much higher levels in DE442 than the wild-type SB1003 strain (Fogg, 2019); we hypothesized that a higher dose of some GafA mutants in DE442 might overcome the impaired RcGTA phenotype and reveal which mutations have the greatest effect on function. Most DE442 *gafA* mutants also failed to complement RcGTA production in gene transfer bioassays, with the exception of L34A and L46A (Fig. 5E). In our alignment, L34 and L46 correspond to *E. coli* DnaA I425 and L438 - neither of which directly bind DNA. In the predicted protein structure L34 is also located on a separate helix to the major groove DNA-binding residues (Fig. 5B). *E. coli* DnaA T435

(equivalent to GafA S43) binds to specific DNA bases and R442 & K443 (GafA R50 & R51) interact with the DNA backbone (Fig. 5A-C) (Fujikawa *et al.*, 2003). DnaA V437 & Q446 (GafA I45 & Q54) are not predicted to bind DNA but they do sit on the same helix as the residues described above and, therefore, mutations in this region may affect the general conformation of the binding site. DnaA R399 & S400 (GafA E8 & S9) bind in the minor groove of DNA (Fujikawa *et al.*, 2003). The AlphaFold model for GafA placed E8 & S9 at a location unlikely to bind DNA (Fig. 5B), however, this could be due to poor multiple sequence alignment coverage at the protein N-terminus (Fig. S3).

Taken together, these data indicate that the truncated GafA-Cx$^{87-382}$ protein can effectively induce expression from the native *gafA* promoter, but full length GafA is required to induce the various other RcGTA loci. It is likely to be the N-terminal DnaA-like DNA binding domain that is essential for activation of the RcGTA promoters.

N- and C-terminal regions of GafA bind DNA

Previous work showed that GafA binds to the RcGTA promoter at a location 75-125 bases upstream of the start codon of TerS (RcGTA *g1*/*rcc01682*) (Fogg, 2019; Sherlock *et al.*, 2019). The C-terminal 162 aa of GafA was expressed from a T7 expression vector with an N-terminal MBP tag. The protein was purified to homogeneity and used for electrophoretic mobility shift (EMSA) assays (Fig. 6). As predicted, MBP-GafA-C$^{221-382}$ bound the RcGTA promoter at the previously identified location (Fig. 6A & B), which contains both the -10 and -35 promoter elements plus the transcription start site (TSS) (Fig. 6A). It is also known that *gafA* binds to its own promoter in a 270 base region upstream from the start codon (Fogg, 2019), however, the precise location was not identified. To refine the binding site, we used three 50 bp Cy5-labelled dsDNA oligos covering 150 bases upstream of the start codon for an EMSA binding assay. GafA-C$^{221-382}$ bound to *gafA* promoter fragment #3, which contains the predicted -35 element (Fig. 6D & E).

Similar protein expression constructs were also made for the GafA-Nc$^{1-86}$ and GafA-N$^{1-226}$ regions with N-terminal His and MBP tags but, as expected, no binding was detected for any DNA targets tested; consistent with data shown in Fig. 4 that N-terminal modifications impair activity of the protein probably by interfering with DNA binding. To resolve this, the affinity purification tag was removed from the MBP-GafA-Nc$^{1-86}$ protein by digestion with 3c protease, and EMSAs were performed with the tag-free protein. GafA-Nc$^{1-86}$ produced DNA mobility shifts consistent with non-specific binding to most templates (Fig. 6). Of the five RcGTA promoter fragments tested, four were bound by GafA-Nc$^{1-86}$ with similar affinities (pGTA #1-4) but only two shifts remained in the presence of an unlabelled non-specific dsDNA competitor (Fig. 6C). The two promoter fragments that produced specific binding were located on either side of the GafA-C$^{221-382}$

binding site (Fig. 6A), which suggests that GafA could bind as a dimer. Analytic gel filtration confirmed that GafA is dimeric in solution, and dimerization is retained for the truncated GafA-Cx$^{87-382}$ and GafA-C$^{221-382}$ proteins (Fig. S6). Of the three *gafA* promoter fragments tested, two were bound by GafA-Nc$^{1-86}$ (pGafA #1 & 2) but neither were specific (Fig. 6F) – consistent with the observation that the GafA N-terminal 86 amino acids are not required for stimulation of the *gafA* promoter.

DISCUSSION

Production of Gene Transfer Agents (GTAs) is indirectly controlled by various global regulators in response to environmental stimuli and the disparate signals are integrated via a single transcription factor, GafA. GafA shares little sequence or structural similarity with proteins of known function, but short regions in the N- and C-termini of the protein have tentative structural similarity to DnaA and sigma factor proteins, respectively (Tables S8-10). These regions of similarity are tightly centred around predicted DNA binding domains. The central portion of GafA, between these putative DNA binding domains, is of unknown function. In this paper we sought to refine the mechanism of action for GafA and to assign functions to the various domains. Interestingly, we have identified a direct interaction between GafA and the RNA polymerase ω sub-unit.

The interaction between GafA and Rpo-ω

Bacterial DNA-dependent RNA polymerase (RNAP) is responsible for the production of all RNA within a given cell. RNAP is a multi-protein holoenzyme comprised of two identical α-subunits, catalytic β and β' sub-units, and an ω sub-unit encoded by the *rpoZ* gene. The Rpo-ω subunit has been studied in a wide variety of species (Kurkela *et al.*, 2021), where it is thought to stabilize the overall RNAP holoenzyme via direct interactions with the β and β' sub-units (Glyde *et al.*, 2018; Lin *et al.*, 2019; Vassylyev *et al.*, 2002). *R. capsulatus* Rpo-ω shares <50% sequence identity with its *E. coli* counterpart, but the MAR ppGpp binding motif and all five conserved residues known to be important for RNAP stabilization are present in both proteins (Kurkela *et al.*, 2021). With the exception of *Mycobacterium tuberculosis* (Mao *et al.*, 2018), deletion of the *rpoZ* gene is not lethal but instead results in various growth defects or alternative phenotypes (Kurkela *et al.*, 2021). Indeed, Westbye *et al.* (2017) showed that the growth rate of *R. capsulatus* Δ*rpoZ* is slower than the wild-type and RcGTA production is abrogated (Westbye *et al.*, 2017), the latter of which was confirmed here (Fig. 1).

Evidence from multiple species indicates that deletion of Rpo-ω decreases transcription of some housekeeping genes and influences global transcription profiles by promoting RNAP preference for alternative sigma factors (Paget, 2015; Shimada *et al.*, 2014; Weiss *et al.*, 2017; Yamamoto *et al.*, 2018). The role of Rpo-ω in sigma factor selection has largely been inferred from transcriptome data showing expression profiles characteristic

of certain sigma factors in wild-type versus Rpo-ω deletion strains, or by the efficiency of sigma factor incorporation into RNAP *in vivo*/*in vitro* (Geertz *et al.*, 2011; Gunnelius *et al.*, 2014; Weiss *et al.*, 2017). Although sigma factors bind to promoter DNA at the -10 and -35 sites, binding is not usually possible *in vitro* in the absence of the RNAP core (Feklístov *et al.*, 2014). Data presented here and elsewhere shows that purified GafA does bind *in vitro* to RcGTA promoters close to the -10/-35 regions (Fig. 6) and that it is the presence of Rpo-ω rather than its absence that leads to expression of GafA regulated genes (Fig. 1) (Fogg, 2019; Westbye *et al.*, 2017). Structural data for RNAP complexes from various species show that the Rpo-ω and sigma factor subunits both primarily interact with Rpo-β' but are spatially separated in the stable holoenzyme (Geertz *et al.*, 2011; Glyde *et al.*, 2018; Mao *et al.*, 2018; Vassylyev *et al.*, 2002; Weiss *et al.*, 2017). Meanwhile transcription factors usually bind upstream of the -35 element and interact with RNAP via the α-subunit (Browning and Busby, 2004). No binding was detected between GafA and the Rpo-α, Rpo-β or Rpo-β' subunits in a bacterial-2-hybrid assay (Fig. 2).

Possible scenarios are: a) GafA first binds to RcGTA promoters and recruits RNAP via an interaction with Rpo-ω; b) GafA pre-recruits RNAP in solution and enhances its affinity for RcGTA promoters, similar to the mechanism thought to be used by the MarA/SoxS family (Griffith *et al.*, 2002; Martin *et al.*, 2002). Perhaps binding to Rpo-ω mimicks the action of ppGpp (Westbye *et al.*, 2017); or c) GafA first binds to Rpo-ω, which then mediates subsequent interactions between GafA and the Rpo-α, β or β' subunits that are not apparent in one-on-one *in vitro* experiments.

Regulation of the RcGTA operons

We have sought to update our previous GafA-centric model for RcGTA (Fogg, 2019) regulation with recent discoveries made here and elsewhere (Fig. 7). An important pre-requisite for RcGTA production is high cell density and transition to stationary phase of growth. The response to cell density is mediated by two contrasting influences - a secreted RTX-domain protein represses expression by an unknown mechanism while a quorum sensing signal molecule (homoserine lactone or HSL) promotes RcGTA gene expression (Brimacombe *et al.*, 2013; Ding *et al.*, 2019; Leung *et al.*, 2012; Westbye *et al.*, 2018). Quorum sensing is also important for regulation of the *Dinoroseobacter shibae* GTA (DsGTA) where deactivation of one HSL synthase abolishes any DsGTA gene expression while disruption of another leads to DsGTA overproduction (Koppenhöfer *et al.*, 2019; Tomasch *et al.*, 2018; Wang *et al.*, 2014). Meanwhile, a RelA/SpoT homologue responds to amino acid starvation by increasing intra-cellular concentrations of (p)ppGpp, which is likely to interact directly with RNAP via Rpo-ω, or an alternative binding site, to alter promoter preference (Westbye *et al.*, 2017). It is worth noting that *Bartonella* GTA (BaGTA) production appears to occur in response to low ppGpp concentration, leading to the hypothesis that BaGTA production actually occurs in the fittest cells in a population

rather than those under the most stress (Québatte and Dehio, 2019; Québatte *et al.*, 2017).

The pleiotropic regulator CtrA is absolutely essential for any detectable RcGTA production, and its phosphorylation state controls the transition from RcGTA assembly and DNA packaging to adornment and lysis (Farrera-Calderon *et al.*, 2021; Lang and Beatty, 2000; Mercer *et al.*, 2010, 2012; Westbye *et al.*, 2013, 2018). Hence effective production and release of mature RcGTA particles is dependent upon an intact phosphorylation cascade from the response regulator CckA to CtrA via ChpT (Farrera-Calderon *et al.*, 2021; Wang *et al.*, 2014; Westbye *et al.*, 2018). High levels of intracellular c-di-GMP stimulate the phosphatase activity of CckA and help to maintain a higher concentration of unphosphorylated CtrA(Farrera-Calderon *et al.*, 2021; Pallegar *et al.*, 2020b, 2020a). In its unphosphorylated state CtrA is required for transcription of *gafA* (Fogg, 2019). Rpo-ω is not required to activate expression of *gafA* and only the C-terminal region of GafA is required for autoregulation (Fig.1 & 4), which indicates that different mechanisms regulate transcription of *gafA* and the core RcGTA structural locus. It is likely that GafA works together with CtrA to recruit RNAP to the *gafA* promoter but works alone at the core RcGTA promoter via interaction with Rpo-ω (Fig. 7) (Fogg, 2019).

Low c-di-GMP levels stimulate CckA kinase activity leading to CtrA phosphorylation(Farrera-Calderon *et al.*, 2021; Pallegar *et al.*, 2020b, 2020a). CtrA-P also increases expression of the PAS domain protein DivL, which further enhances CckA kinase activity (Fogg, 2019; Westbye *et al.*, 2018). CtrA-P then acts in concert with GafA to trigger the various late stage RcGTA genes – head spike (*rcc01079/80* aka *ghsA/B*), tail fibres (*rcc00171*) and lysis genes (*rcc00555*/*6*) (Fogg, 2019). Putative CtrA half sites were detected in the promoters of all three of these loci and putative GafA binding sites in two out of three (Fig. S7). The housekeeping protease ClpXP degrades both forms of CtrA and is important for maintenance of a proper equilibrium of phosphorylation states (Westbye *et al.*, 2018). Interestingly, deletion of ClpX leads to tailless immature RcGTA particles, reminiscent of DNA packaging mutants(Sherlock *et al.*, 2019).

The overall model presented here appears to be mostly complete, with a few notable exceptions. The SoS response regulator LexA is required for RcGTA production but its precise mechanism is unknown, although it appears to act via CckA (Kuchinski *et al.*, 2016). There is an SoS box in the LexA promoter and deletion of *lexA* leads to increased expression of *cckA*. This dysregulation presumably unbalances CtrA phosphorylation and/or degradation. Notably, LexA, c-di-GMP, CckA and the phosphorylation of CtrA are all associated with the regulation of DsGTA (Koppenhöfer *et al.*, 2019), but more work is required to fully determine common mechanisms between the species. Another enigmatic protagonist is *rcc01866*, which is located adjacent to the *gafA* gene and is expressed divergently. The Δ*1866* mutant has a phenotype similar to Δ*cckA* i.e. RcGTA particles are

produced but are not fully mature and no detectable lysis occurs (Hynes *et al.*, 2016). We were unable to predict any putative function for the 1866 protein by primary sequence similarity or structural homology searches.

The *gafA* genes beyond the Rhodobacterales

Through bioinformatics analysis, we have identified *gafA* regions with conserved local synteny in the Hyphomicrobiales Order (Fig. S2 & Table S1B-F). The *gafA* homologues are found in a wide variety of species throughout the Order including several important pathogens such as those from the *Brucella* (Chain *et al.*, 2011) and *Agrobacterium* genera (Scholz *et al.*, 2008). The *Brucella gafA* genes have also previously been implicated as virulence/fitness factors of unknown function in high-throughput studies (He, 2012; Salmon-Divon *et al.*, 2019). Intriguingly, the Hyphomicrobiales *gafA* is split into two separate genes that roughly correspond to the GafA-Nc and GafA-Cx constructs used in this study, supporting the hypothesis that these domains have distinct biological roles.

Overall our data suggest that GafA either acts as an alternative sigma factor or as a transcription factor that is recruited by Rpo-ω via a direct protein:protein interaction (Lane and Darst, 2006; Lin *et al.*, 2019; Li *et al.*, 2019), and this interaction occurs via the central domain of the protein (Fig. 2 & 3). GafA has two mechanisms of action, one Rpo-ω dependent and one Rpo-ω independent, and the GafA N-terminal DNA binding domain is essential only for the former. Further research is ongoing to determine the precise mechanism of GafA and to establish how widespread this mechanism is in bacteria.

Limitations of the study

The DNA sequence bound by GafA was predicted from the short regions of the GafA and RcGTA promoters identified by EMSA analysis, however, a more extensive experimental approach will be required to confirm and refine these predictions e.g. systematic DNA mutagenesis. Although we demonstrated that GafA interacts with RNAP via the Omega sub-unit to co-ordinate RcGTA expression, we did not present a definitive mechanism for how RNAP promoter preference is altered. We envisage that this will be resolved via biochemical/structural approaches for the whole RNAP holoenzyme in complex with GafA and DNA.

Author Contributions

Conceptualization, P.C.M.F; Methodology, D.S. and P.C.M.F.; Investigation, D.S. and P.C.M.F.; Writing, P.C.M.F.; Visualization, P.C.M.F.; Funding Acquisition, P.C.M.F.; Resources, P.C.M.F.; Supervision, P.C.M.F.

Acknowledgements

We would like to thank Prof. Thomas Beatty (University of British Columbia) for critical reading of the manuscript and for his astute suggestion for the GafA-C DNA binding site. We would also like to thank Dr Alexander Westbye (Oslo University Hospital) for critical reading of the manuscript and insightful comments. We acknowledge the important contributions of equipment/technical support from the Genomics and Molecular Interactions labs at the University of York Technology Facility. This research was funded by a Wellcome Trust & Royal Society Sir Henry Dale Independent Research Fellowship Grant (109363/Z/15/A) and a Biotechnology and Biological Sciences Research Council responsive mode grant (BB/V016288/1) awarded to Dr Paul Fogg.

Declaration of Interests

The authors declare no competing interests

Figure Titles and Legends

Figure 1. The *rpoZ* gene is essential for RcGTA production. For all panels the following strains were used – *R. capsulatus* SB1003 (WT) and a *rpoZ* KO derivative (ΔrpoZ*)*. Strains were complemented *in trans* with empty pCM66T vector (WT and ΔrpoZ), *rpoZ* expressed from its native promoter (+*rpoZ*), *gafA* expressed from its native promoter (+gafA), or *gafA* overexpressed from a cumate inducible promoter (+*gafA* OX). **A.** Representative western blot of *R. capsulatus* concentrated supernatants using an α-RcGTA capsid antibody. **B.** Bar chart showing the frequency of rifampicin gene transfer by the indicated strains, N=6. **C.** Quantitative PCR data showing *gafA* transcript abundance in the indicated strains relative to the *R. capsulatus* SB1003 (WT) control. Expression levels shown were calculated using the ΔΔCt method (*uvrD* reference gene) and a log2 transformation to give fold-differences. N=3. **D.** Bar chart of the frequency of rifampicin gene transfer by the annotated strains. N=4. Statistical significance is indicated on each graph as calculated by one-way ANOVA with the Holm-Sidak method for pairwise multiple comparison (***= p<0.001, **= p<0.01, *= p<0.05, n.s.= p>0.05). See also Data S1.

Figure 2. GafA directly interacts with Rpo-ω. A. Quantification of bacterial-2-hybrid interactions between T25-GafA vs T18-Rpo-α, T18-Rpo-β, T18-Rpo-β' and T18-Rpo-ω. Negative control is T25-gafA vs pUT18 empty vector (-ve). N=3. Statistical significance is indicated on the graph as calculated by one-way ANOVA with the Holm-Sidak method for pairwise multiple comparison (***= p<0.001). **B.** Silver stained SDS PAGE gel of a pull-down assay using MBP-GafA as bait and H6-Rpo-ω as prey. Amylose magnetic beads that should only bind to MBP-tagged proteins were used to capture the proteins. Presence or absence of each protein in the assay is indicated by '-' or '+' symbols above the gel. Abcam broad range protein marker is included for reference. See also Data S1.

Figure 3. The domain structure of the *R. capsulatus* GafA. A. Amino acid sequence of GafA, colour coded to highlight the different regions used for subsequent characterization. Green = N-terminal concise (Nc, residues 1-86), Green & Blue = N-terminal (N, residues 1-226), Turquoise = C-terminal (C, residues 221-382), Blue-Turquoise = C-terminal extended (Cx, residues 87-382), Blue = Central region 2 (Cen2, residues 87-212), Blue & Purple = Central region N (CenN, residues 87-226). **B.** Alphafold structure prediction for GafA, regions used for subsequent characterization are colour coded as in part A and annotated above and below the image. The two predicted DNA binding domains (DBD) are annotated with arrows. **C.** Quantification of bacterial-2-hybrid interactions between T18-Rpo-ω and various T25-GafA constructs (defined above) by β-galactosidase assay, N=3. Statistical significance is indicated on the graph as calculated by one-way ANOVA with the Holm-Sidak method for pairwise multiple comparison (***= p<0.001, n.s.= p>0.05). **D.** InstantBlue stained SDS PAGE gel of a pull-down assay using MBP-GafA-Cx as bait and H6-Rpo-ω as prey. Amylose magnetic beads were used to capture the proteins. Presence or absence of each protein in the assay is indicated by '-' or '+' symbols above the gel. Abcam broad range protein marker and a lane showing the Rpo-ω protein input are included for reference. See also Figure S1-4, Table S1 & 2, Data S1.

Figure 4. Characterization of GafA domain function. A-C. Bar charts of the relative frequency of rifampicin gene transfer from **A.** *R. capsulatus* SB1003 wild-type donor strains complemented *in trans* with empty pQF vector (WT), full length *gafA* (Σ), or truncated regions of *gafA* described in Fig. 3 (N, C and Cx), N = 3. **B.** *R. capsulatus* SB1003 wild-type donor strains complemented *in trans* with empty pCM66T vector (WT, N=3) or with the *puf* promoter driving expression of full length *gafA* (Σ, N=4), or truncated regions of *gafA* (Nc and N, N=4) or **C.** *R. capsulatus* SB1003 Δ*gafA* donor strains complemented *in trans* with empty pCM66T vector (WT, N=8) or with the *puf* promoter driving expression of full length *gafA* (Σ, N=4), or truncated regions of *gafA* (Nc and N, N=7). **D.** Transcript abundance of RcGTA genes in *gafA* overexpression strains. The bar chart shows relative changes in transcript abundance measured using quantitative PCR and the ΔΔCt method. The *R. capsulatus* strains tested are annotated in the legend – SB1003 containing empty pQF (WT), SB1003 complemented with pCMF254 (WT + *gafA* OX), SB1003 complemented with pCMF264 (WT + *gafA* Cx OX) and SB1003 *gafA* knock-out complemented with pCMF264. Transcripts of *gafA*, RcGTA capsid (*rcc01687*), RcGTA endolysin (*rcc00555*) and the *gafA* 5' UTR (*pGafA*) were measured. Statistical significance for all panels is indicated above each graph, and was calculated by one-way ANOVA with the Holm-Sidak method for pairwise multiple comparison (***= $p<0.001$, n.s.= $p>0.05$). See also Figure S5.

Figure 5. Mutagenesis of the GafA N-terminal DNA binding domain. A. Alignment of *R. capsulatus* GafA (Rc_GafA) residues 1-59 with the DnaA DNA binding domains from *E. coli* (PDB: 1J1V), *Mycobacterium tuberculosis* (PDB: 3PVV), *Aquifex aeolicus* (PDB: 1L8Q) and *R. capsulatus* (Rc_DnaA). Conserved amino acids are coloured using the CLUSTLx scheme and mutated positions are indicated by black boxes. **B.** Alphafold structure prediction for the GafA N-terminal DNA binding domain. Side chains are shown for the amino acid positions mutated in this study, and each are coloured according to predicted interaction with DNA; Red – specific base interaction, Blue – nonspecific interaction with DNA backbone, Green – no direct interaction. **C.** DNA binding domain from *E. coli* DnaA (PDB: 1J1V). Equivalent amino acids to those mutated in GafA are coloured using the same scheme as in panel B. R399 and S400 are annotated as they sit in the minor groove of DNA, whereas their GafA counterparts (E8/S9) were predicted to have no proximity to the DNA – probably due to limitations of the model at the sequence extremity. **D & E.** Relative gene transfer frequencies for *gafA* gene knock-outs of **D** the wild-type strain *R. capsulatus* SB1003 (N=4, except E8 where N=3) and **E** the RcGTA overproducer strain DE442 (N=4, except S9 where N=3). Each strain was complemented *in trans* with either empty pCM66T vector (Δ) or the *gafA* gene with single point mutations as indicated on the X-axis. Frequencies shown are normalized to complementation of the respective strains (SB1003 or DE442) with unmodified *gafA*. Statistical significance tested by one-way ANOVA with the Holm-Sidak method for pairwise multiple comparison – all *gafA* point mutations were statistically different from wild-type *gafA* ($p<0.001$) except DE442 complemented with *gafA* L34A or L46A ($p>0.05$).

Figure 6. Binding of GafA domains to the RcGTA and *gafA* promoters. A. Schematic of the RcGTA promoter region with the start codon (ATG), transcription start site (TSS) and -10/-35 promoter elements annotated. The locations of DNA fragments used for EMSA band shifts are shown and labelled #1 to #4. **B.** Representative EMSA of GafA-$C^{221-382}$ binding to RcGTA promoter fragment #2. **C.** Representative EMSA of GafA- Nc^{1-86} binding specifically to RcGTA

promoter fragments #1 & 3 and non-specifically to #2 & 4. Protein concentration is labelled above the image. N = excess of non-specific competitor DNA added, S = excess of specific competitor DNA added. **D.** Schematic of the *gafA* promoter region with the start codon (ATG), transcription start site (TSS), CtrA binding site (CtrA) and -10/-35 promoter elements annotated. The locations of DNA fragments used for EMSA band shifts are shown and labelled #1 to #3. **E.** Representative EMSA of GafA-$C^{221-382}$ binding to *gafA* promoter fragment #3. **F.** Representative EMSA of GafA-Nc^{1-86} binding non-specifically to *gafA* promoter fragments #1 & 2. Protein concentration is labelled above the image. N = excess of non-specific competitor DNA added, S = excess of specific competitor DNA added. See also Figure S6&7.

Figure 7. Model of RcGTA regulation. Known contributors to RcGTA regulation are indicated and broadly classified based on whether their major influence is on early production of structural proteins (Stage 1) or late stage maturation and lysis (Stage 2). Arrows indicate positive regulation and flat headed arrows indicate repression. Black arrows represent transcriptional regulation, blue arrows represent post-translational or ligand:protein regulation, red arrows represent biosynthesis or degradation, dashed arrows indicate uncertain mechanism. Arrows representing GafA regulation that requires Rpo- ω are annotated with 'ω', and Rpo- ω independent regulation by the GafA Cx domain is labelled 'Cx'.

STAR Methods

RESOURCE AVAILABILITY

Lead contact

Further information and requests for resources and reagents should be directed to and will be fulfilled by the lead contact, Paul Fogg (paul.fogg@york.ac.uk).

Materials availability

All unique reagents or materials generated in this study will be made available on request by the lead contact, but we may require a completed materials transfer agreement if there is potential for commercial application.

Data and code availability

- All data reported in this paper will be shared by the lead contact upon request
- This paper does not report original code
- Any additional information required to reanalyze the data reported in this paper is available from the lead contact upon request.

EXPERIMENTAL MODEL AND SUBJECT DETAILS

Bacterial Strains

Three *Rhodobacter capsulatus* strains were used in this study: rifampicin sensitive wild-type strain B10 (Wall *et al.*, 1975), a rifampicin resistant derivative SB1003 (ATCC BAA-309) and an RcGTA overproducer strain DE442 (Ding *et al.*, 2014; Fogg *et al.*, 2012). All *R. capsulatus* cultures were grown at 30°C either aerated in the dark or in anoxic sealed tubes under constant illumination. Two growth media were used – YPS complex broth (0.3 % w/v yeast extract, 0.3% w/v peptone, 2 mM $MgCl_2$, 2 mM $CaCl_2$) or RCV defined broth (10 mM potassium phosphate buffer, 0.4% w/v L-malic acid, 0.1% w/v $(NH_4)_2SO_4$, 0.020% w/v $MgSO_4{\cdot}7H_2O$, 0.0075% w/v $CaCl_2{\cdot}2H_2O$, 0.0012% w/v $FeSO_4{\cdot}7H_2O$, 0.0020% w/v Na_2EDTA, 0.0001% w/v thiamine hydrochloride. Plus 1 ml of trace element solution - 0.07% w/v H_3BO_3, 0.040% w/v $MnSO_4{\cdot}H_2O$, 0.019% w/v $Na_2MoO_4{\cdot}2H_2O$, 0.006% w/v $ZnSO_4{\cdot}7H_2O$, 0.001% w/v $Cu(NO_3){\cdot}3H_2O$. The pH was adjusted to 6.8 with NaOH). For agar plates, 1.5% w/v agar was added to the above broth recipes. The *E. coli* S17-1 strain (DSM 9079), which contains chromosomally integrated *tra* genes, was used as a donor for all conjugations. NEB 10-beta Competent *E. coli* cells (New England Biolabs) were used for standard cloning and plasmid maintenance; T7 Express

Competent *E. coli* cells (New England Biolabs) were used for overexpression of proteins for purification.

METHOD DETAILS

Plasmid Construction

Cloning and Site Directed Mutagenesis

A full list of all plasmids and oligonucleotides used in the study can be found in Tables S3 and S4. All oligonucleotides were obtained from Integrated DNA Technologies (IDT) and designed with an optimal annealing temperature of 60°C when used with Q5 DNA Polymerase (New England Biolabs). Plasmid DNA was purified using the Monarch Plasmid Miniprep Kit (New England Biolabs). The destination plasmids pCM66T, pKT25, pUT18 and pUT18C were linearized by digestion with BamHI restriction enzyme (New England Biolabs), pETFPP_1 & 2 was linearized by PCR using inverse primers CleF and CleR. Inserts were amplified using primers with 15 bp 5' overhangs that have complementary sequence to the plasmid DNA with which it was to be recombined. All cloning reactions were carried out with the NEBuilder Cloning Kit (New England Biolabs). Site-directed mutagenesis was achieved by inverse PCR using Q5 DNA polymerase overlapping primers (offset by 8 to 10 bp) containing the desired mutation in the centre of the overlap region. Amplified DNA was cleaned using the Monarch PCR & DNA Cleanup Kit (New England Biolabs), then digested with DpnI restriction endonuclease (New England Biolabs) overnight at 37°C and introduced without further treatment into chemically competent *E. coli* by transformation.

Transformation and conjugation

Plasmids were introduced into *E. coli* by standard heat shock transformation (Maniatis *et al.*, 1982), and into *Rhodobacter* by conjugation. One millilitre aliquots of overnight cultures of the *E. coli* S17-1 donor and *Rhodobacter* recipient strains were centrifuged at 5,000 x g for 1 min, washed with 1 ml YPS broth, centrifuged again and resuspended in 100 µl YPS broth. 10 µl of concentrated donor and recipient cells were mixed and spotted onto YPS agar or spotted individually as negative controls. Plates were incubated o/n at 30°C. Spots were scrapped, suspended in 100 µl YPS broth and plated on YPS + 100 µg/ml rifampicin (counter-selection against *E. coli*) + 10 µg/ml kanamycin or 1 µg/ml tetracycline (plasmid selection). Plates were incubated o/n at 30°C then restreaked onto fresh selective agar to obtain pure single colonies.

Gene Knockouts

Knockouts were created by RcGTA transfer. pCM66T plasmid constructs were created with a gentamicin resistance cassette flanked by 500-1000 bp of DNA from either side of the target gene. Assembly was achieved by a one-step, four component NEBuilder (NEB) reaction and transformation into NEB 10-beta cells. Deletion constructs were introduced into the RcGTA hyperproducer strain and a standard GTA bio-assay (see below) was carried out to replace the intact chromosomal gene with the deleted version.

Rhodobacter Gene Transfer Assays

Rhodobacter assays were carried out essentially as described in (Leung and Beatty, 2013). RcGTA donor cultures were grown photosynthetically (anoxic) with illumination in YPS for ~72 h and recipient cultures were grown under chemotrophic conditions in RCV for ~24 h. Cells were cleared from donor cultures by centrifugation and the supernatant filtered through a 0.45 µm syringe filter. Recipient cells were concentrated 3-fold by centrifugation at 5,000 x g and resuspension in 1/3 volume of G-Buffer (10 mM Tris-HCl pH 7.8, 1 mM $MgCl_2$, 1 mM $CaCl_2$, 1 mM NaCl, 0.5 mg/ml BSA). Reactions were carried out in polystyrene culture tubes (Starlab) containing 400 µl G-Buffer, 100 µl recipient cells and 100 µl filter donor supernatant, then incubated at 30°C for 1 h. 900 µl YPS was added to each tube and incubated for a further 3 h. Cells were harvested by centrifugation at 5,000 x g and plated on YPS + 100 µg/ml rifampicin (for standard GTA assays) or 3 µg/ml gentamicin (for gene knock-outs).

Nucleic Acid Purification

One millilitre samples of relevant bacterial cultures were taken for each nucleic acid purification replicate. Total DNA was purified according to the "Purification of Nucleic Acids by Extraction with Phenol:Chloroform" protocol (Maniatis *et al.*, 1982). Cells were resuspended in 567 µl TE then 30 µl 10% (w/v) SDS and 3 µl 20 µg/ml Proteinase K were added. Cells were incubated at 37°C for 1 h. To each tube, 100 µl of 5 M NaCl was added and thoroughly mixed by inversion. Eighty microlitres of 1% (w/v) CTAB was added, mixed thoroughly by inversion and the cells were incubated at 65°C for 10 minutes. An equal volume of Phenol:chloroform:isoamyl alcohol (25:24:1, pH 8) was added and mixed vigorously. The tubes were centrifuged at 15,000 x g for 10 min. The upper aqueous layer was removed to a fresh tube and the Phenol:chloroform:isoamyl alcohol treatment was repeated at least two times or until the white interphase was no longer visible. An equal volume of chloroform was added and mixed vigorously. The tubes were centrifuged at 15,000 x g for 2 min. The upper aqueous layer was transferred to a fresh tube and DNA was precipitated by addition of 0.6 volumes of ice-cold isopropanol. Precipitation was allowed to proceed at -20°C for 1 h. DNA was harvested by centrifugation at 15,000 x g for 15 min, and the supernatant was discarded. The pellet was washed with 70% ethanol, centrifuged at 15,000 x g for 15 min and the supernatant was discarded. The pellet was

allowed to air dry for ~15 min then resuspended in TE buffer. Total RNA was purified using the NucleoSpin RNA Kit (Macherey-Nagel) and DNAseI treated on column according to the recommended protocol. RNA was quantified using a Nanodrop spectrophotometer. 1 µg of total RNA was converted to cDNA using the LunaScript RT SuperMix Kit (NEB).

Quantitative Reverse Transcriptase PCR

One in fifty dilutions of the cDNA template were prepared and 1 µl used per reaction. Reactions contained Fast Sybr Green Mastermix (Applied Biosystems), cDNA and primers (500 nM). Standard conditions were used with an annealing temperature of 60°C. All primer efficiencies were calculated as between 90 and 110%. Relative gene expression was determined using the ΔΔCt method (Livak and Schmittgen, 2001). For each sample, variance was calculated for three independent biological replicates, which were each the mean of three technical replicates. QuantStudio 3 Real-Time PCR System was used for all experiments (Applied Biosystems).

GafA Overexpression in *Rhodobacter*

Gene overexpression in *Rhodobacter* was achieved by a transcriptional fusion of the genes of interest to a cumate inducible promoter in the plasmid pQF (Kaczmarczyk *et al.*, 2013) or to the *R. capsulatus puf* photosynthesis promoter in pCM66T (Fogg, 2019; Fogg *et al.*, 2012). For overexpression experiments using the *puf* promoter, donor cultures were first grown chemotrophically in the presence of oxygen to stationary phase then diluted 1:1 in fresh media and switched to anoxic photosynthetic growth for 6 h. pQF was a gift from Julia Vorholt (Addgene plasmid #48095). Overexpression was induced by addition of cumate to late log growth phase cultures at a final concentration of 50 µM.

Bacterial-two-hybrid (B2H) assays

The procedure and the resources were as described in (Karimova *et al.*, 1998). Plasmids encoding T18 (pUT18C and derivatives) and the compatible plasmids encoding T25 (pKT25 and derivatives) were introduced pairwise into competent BTH101 by co-transformation. Selection was using LB agar containing 50 µg/ml kanamycin, 100 µg/ml ampicillin, 1 mM IPTG and 80 µg/ml X-Gal, and plates were incubated at 30°C for 48 h to allow blue colour to develop. Colonies obtained from the B2H plate assay were used to inoculate 5 ml of LB supplemented with 50 µg/ml kanamycin, 100 µg/ml ampicillin and 1 mM IPTG in a 96-well plate. Plates were incubated for 16 h at 30°C with agitation. Absorbance (OD_{600}) readings of culture density were taken. Meanwhile, 80 µl aliquots of permeabilization solution (100 mM Na_2HPO_4, 20 mM KCl, 2 mM $MgSO_4$, 0.5 mg/ml lysozyme) were mixed with 20 µl of each bacterial culture, then incubated at room temperature for 30 min. Six hundred microliters of substrate solution (60 mM Na_2HPO_4,

40 mM NaH_2PO_4, 1 mg/ml ONPG) was added and the mixture was incubated at room temperature. Once sufficient colour had developed, stop solution (1 M sodium carbonate) was added and the precise time noted. Cell debris was removed by centrifugation and absorbance (OD_{420}) readings were taken. Miller units were calculated according to the formula MU=1,000(Abs420/(Abs600*0.02 ml*time in min)).

Protein Purification

For His6-tagged proteins, 500 ml cultures of *E. coli* containing the relevant expression plasmid were induced at mid-exponential growth phase with 0.2 mM IPTG overnight at 20°C (Fogg and Wilkinson, 2008). Concentrated cells were lysed in 20 ml binding buffer (0.5 M NaCl, 75 mM Tris; pH 7.75) plus 0.2 mg ml^{-1} lysozyme and 500 U Basemuncher Endonuclease (Expedeon Ltd.) for 30 min on ice and then sonicated. Cleared supernatant was applied to a 5 ml HisTrap FF crude column (Cytiva) and the bound, his-tagged protein was eluted with 125 mM imidazole. Eluted protein was desalted on a HiPrep 26/10 desalting column (Cytiva) and then further separated by size exclusion chromatography on a HiLoad 16/60 Superdex 200 preparative grade gel filtration column. All chromatography steps were carried out on an AKTA Prime instrument (Cytiva). Purified proteins were concentrated in a Spin-X UF Centrifugal Concentrator (Corning) and quantified by the nanodrop extinction co-efficient method (Thermo Scientific). Samples were stored at -80 °C in binding buffer plus 50% glycerol. MBP-tagged proteins were purified as above except MBP binding buffer was used (200 mM NaCl, 20 mM Tris, 1 mM EDTA; pH 7.4), the lysate was applied to a 5 ml MBPTrap FF column (Cytiva) and purified protein was eluted with 10 mM maltose in binding buffer.

Analytical Gel Filtration

Protein multimeric states were estimated using a Superdex 200 increase 10/200 GL column (Cytiva). MBP binding buffer was used for all filtration runs. A protein molecular weight standard (1.3–670 kDa, Bio-Rad Laboratories) was run through the column at 0.75 ml/min and the peaks produced were used to construct a standard curve (R^2=1, predicted error for 17-670 kDa is <2%). Samples of each protein were sequentially run on the column and molecular weights were estimated from the elution volume and the equation derived from the standard curve.

Electrophoretic motility shift assays (EMSA)

For all 50 bp binding substrates, 50 base Cy5 5'-labelled oligos (IDT) were annealed to unlabelled complimentary oligos (IDT). Both oligos were mixed to a final concentration of 40 µM in annealing buffer (1 M Potassium Acetate, 300 mM HEPES; pH 7.5) and heated to 98°C for 5 min then allowed to cool to room temperature. Ten microliter EMSA mixtures contained 80 nM annealed Cy5-dsDNA, standard binding buffer (25 mM HEPES, 50 mM

K-glutamate, 50 mM $MgSO_4$, 1 mM dithiothreitol, 0.1 mM EDTA, 0.05% Triton X-100; pH 8.0) (Wiethaus *et al.*, 2008), 1 µg poly dI:dC, 4% glycerol and the specified concentrations of purified protein (Wiethaus *et al.*, 2006). 500-fold excess of competitor DNA was added to control mixtures – specific competitor was unlabelled but otherwise identical to the binding substrate and the non-specific competitor was an unlabelled 50 bp annealed oligo matching an arbitrary location elsewhere in the *R. capsulatus* genome. All assays were incubated for 30 min at room temperature then immediately loaded onto a 7 % Acrylamide gel (1 x TBE) without loading dye. Gels were run at 80 V for 90 min at room temperature in 1 x TBE. Fluorescence was imaged using a Typhoon Biomolecular Imager (Amersham) and analysed using ImageQuant (Amersham) and FIJI (Schindelin *et al.*, 2012) software.

Protein ligand pull down assays

One hundred microliters of 2 mg/ml MBP-tagged protein in binding buffer (200 mM NaCl, 20 mM Tris, 1 mM EDTA; pH 7.4) was incubated with 100 µl of amylose magnetic beads (New England Biolabs) at 4°C for 1 hour on a rolling platform. Mock beads were created by an identical method but using 100 ul of binding buffer without protein. Beads were washed 5 times with 500 µl of wash buffer (binding buffer + 0.05% Tween20) and resuspended in a final volume of 100 µl. For pull downs, 25 µl of prepared beads were harvested in a magnetic stand and the supernatant was replaced with either 100 µl of binding buffer alone or binding buffer containing 2 mg/ml H6-RpoZ. The beads were incubated for 2 h at 4°C on a rolling platform, then washed five times with wash buffer. To elute proteins, 50 µl of elution buffer was added (binding buffer + 10 mM maltose). LDS buffer (Abcam) was added to the eluate and heated to 90°C for 10 min. Twenty microliters of each sample were run on a 4-20% TruPAGE denaturing gradient gel (Merck Life Science Ltd) and the bands were visualized using Pierce silver stain for mass spectrometry (Thermo Scientific) or InstantBlue Coomassie stain (Abcam). Five microliters of extra broad molecular weight prestained protein ladder was used for size estimation (Abcam).

Western Blotting

Rhodobacter capsulatus supernatants were concentrated 10-fold using a SpeedVac (Thermo Scientific). Fifteen microliter samples were mixed with 5 µl LDS sample buffer (Abcam). heated to 90°C for 10 min and then run on 4-20% TruPAGE denaturing gradient gel (Merck Life Science Ltd). Proteins were transferred to a PVDF membrane using a Mini-PROTEAN Tetra Cell blotting module (Bio-Rad Laboratories) in 1X transfer buffer (25 mM tris base, 0.2 M glycine, 20% methanol; pH8.5), 100 V for 1 h. The membrane was blocked in 5% (w/v) skimmed milk powder in 1X TBS for 1 h at room temperature. The anti-RcGTA major capsid protein antibody (Agrisera Ltd) was used at 1:1000 dilution in blocking buffer overnight at 4°C, followed by four 10 min washes in TBST. The

secondary HRP-antibody conjugate was used at 1:2500 dilution in blocking buffer for 2 h at room temperature, followed by four 10 min washes in TBST. SuperSignal west femto maximum sensitivity substrate (Thermo Scientific) was used to develop the western and the signal was detected using an iBRIGHT chemi-imager (Thermo Scientific).

Sequence similarity analysis

NCBI BLASTp and PSI-BLAST searches for GafA homologues were performed using the default parameters - expect threshold=0.05, word size=6 or 3 (respectively), blosum62 similarity matrix, gap costs of existence=11 and extension=1. Queries were made against the non-redundant protein sequences database (nr; posted:May 5th 2022). Where indicated, taxonomic constraints were applied to limit results to the Hyphomicrobiales (taxid:356), Brucellaceae (taxid:118882) and Agrobacterium (taxid:357). A tBLASTn search was made using a GafA homologue from Roseibium sp. RKSG952 as a query and using the default parameters - expect threshold=0.05, word size=6, blosum62 similarity matrix, gap costs of existence=11 and extension=1. The nucleotide collection database was used (nr/nt; May 9th 2022 update). A summary of the full outputs can be found in Table S1.

HHPRED analysis of GafA was carried out using the "pdb_mmcif70_14_Apr" and "NCBI_Conserved_Domains(CD)_v3.18" databases accessed on the 8th May 2022 (Gabler *et al.*, 2020; Zimmermann *et al.*, 2018). Full length GafA protein sequence and two shorter sequences, focused on the two predicted DNA binding domains, were used as queries. The default parameters were used in each case i.e. HHBlits UniRef30 MSA generation method, maximal generation steps = 3 and an E-value threshold of 1e-3. Minimum coverage was 20%, minimum sequence identity was 0%. Secondary structure scoring was done during alignment. A summary of the full outputs can be found in Table S2.

Protein structure and function prediction

Three-dimensional structures for the *R. capsulatus* GafA and Rpo-ω proteins were predicted using the Alphafold co-lab server using the msa_method:jackhammer and all other parameters set to default (Jumper *et al.*, 2021). GafA predictions were made on 30th Sept 2021 and RpoZ predictions were made on 3rd February 2022. Protein structures were visualized using the UCSF ChimeraX version 1.1 (Goddard *et al.*, 2018). Protein:protein interaction predictions were produced using the LZerD protein docking algorithm on the LZerD web server using default parameters (Christoffer *et al.*, 2021). Helix-turn-helix predictions were carried out using NPS@ (Combet *et al.*, 2000; Dodd and Egan, 1990) and Gym2.0 (Narasimhan *et al.*, 2002) using the default settings. Promoter -10/-35 elements were predicted with BPROM (Solovyev and Salamov, 2011). Clustal-ω (Sievers *et al.*, 2011) was used for DNA/protein alignments and Jalview version: 2.11.2.2

(Waterhouse *et al.*, 2009) was used to visualize these alignments; relevant similarity/identity colour schemes are indicated in the figure legends.

QUANTIFICATION AND STATISTICAL ANALYSIS

CorelDraw 2018 (Corel Corporation) was used for figure preparation Statistical analysis was carried out using Sigmaplot software version 13 (Systat Software Inc.) and, for each use, the test parameters are indicated in the figure legends and, where appropriate, in the main text. All graphs present the means as a bar chart and the individual data points are overlaid as discrete dots. All N values quoted refer to distinct biological replicates.

SUPPLEMENTAL ITEM TITLES AND LEGENDS

Table S1. Full BLAST search results for **S1A** *R. capsulatus* SB1003 GafA full length protein query (BLASTp), **S1B** *R. capsulatus* SB1003 GafA full length protein query (BLASTp; hits limited to Hyphomicroberales), **S1C** *R. capsulatus* SB1003 GafA full length protein query (PSI-BLAST - 2 iterations; hits limited to Hyphomicroberales), **S1D** *Roseibium sp. RKSG952* GafA full length protein query (tBLASTn), **S1E** *R. capsulatus* SB1003 GafA full length protein query (BLASTp; hits limited to *Agrobacteria*), and **S1F** *R. capsulatus* SB1003 GafA full length protein query (BLASTp; hits limited to Brucellaceae). Related to Figure 3 and STAR methods.

Table S2. Full HHPRED search results for **S2A** full length *R. capsulatus* SB1003 RpoZ query, **S2B** full length *R. capsulatus* SB1003 GafA query, **S2C** *R. capsulatus* SB1003 GafA N-terminal DNA-binding domain query, and **S2D** *R. capsulatus* SB1003 GafA C-terminal DNA-binding domain query. Related to Figure 3 and STAR methods.

Table S3. A complete list of all plasmids used in this study. Related to STAR methods.

Table S4. A complete list of all oligonucleotides used in this study. Related to STAR methods.

Data S1. Uncropped western blots, SDS PAGE and agarose gel images. Related to Figures 1, 2, 3 and S5.

References

Berglund, E.C., Frank, A.C., Calteau, A., Vinnere Pettersson, O., Granberg, F., Eriksson, A.-S., Näslund, K., Holmberg, M., Lindroos, H., and Andersson, S.G.E. (2009). Run-off replication of host-adaptability genes is associated with gene transfer agents in the genome of mouse-infecting *Bartonella grahamii*. PLoS Genet. *5*, e1000546.

Blaesing, F., Weigel, C., Welzeck, M., and Messer, W. (2000). Analysis of the DNA-binding domain of *Escherichia coli* DnaA protein. Mol. Microbiol. *36*, 557–569.

Brimacombe, C.A., Stevens, A., Jun, D., Mercer, R., Lang, A.S., and Beatty, J.T. (2013). Quorum-sensing regulation of a capsular polysaccharide receptor for the *Rhodobacter capsulatus* gene transfer agent (RcGTA). Mol. Microbiol. *87*, 802–817.

Browning, D.F., and Busby, S.J. (2004). The regulation of bacterial transcription initiation. Nat. Rev. Microbiol. *2*, 57–65.

Chain, P.S.G., Lang, D.M., Comerci, D.J., Malfatti, S.A., Vergez, L.M., Shin, M., Ugalde, R.A., Garcia, E., and Tolmasky, M.E. (2011). Genome of *Ochrobactrum anthropi* ATCC 49188 T, a versatile opportunistic pathogen and symbiont of several eukaryotic hosts. J. Bacteriol. *193*, 4274–4275.

Christoffer, C., Bharadwaj, V., Luu, R., and Kihara, D. (2021). LZerD Protein-Protein docking webserver enhanced with *de novo* structure prediction. Front. Mol. Biosci. *8*, 724947.

Combet, C., Blanchet, C., Geourjon, C., and Deléage, G. (2000). NPS@: network protein sequence analysis. Trends Biochem. Sci. *25*, 147–150.

Ding, H., Moksa, M.M., Hirst, M., and Beatty, J.T. (2014). Draft genome sequences of six *Rhodobacter capsulatus* strains, YW1, YW2, B6, Y262, R121, and DE442. Genome Announc. *2*.

Ding, H., Grüll, M.P., Mulligan, M.E., Lang, A.S., and Beatty, J.T. (2019). Induction of *Rhodobacter capsulatus* gene transfer agent (RcGTA) gene expression is a bistable stochastic process repressed by an extracellular calcium-binding RTX protein homologue. J. Bacteriol. *201*, e00430-19.

Dodd, I.B., and Egan, J.B. (1990). Improved detection of helix-turn-helix DNA-binding motifs in protein sequences. Nucleic Acids Res. *18*, 5019–5026.

Dove, S.L., and Hochschild, A. (1998). Conversion of the omega subunit of *Escherichia coli* RNA polymerase into a transcriptional activator or an activation target. Genes Dev. *12*, 745–754.

Esterman, E.S., Wolf, Y.I., Kogay, R., Koonin, E.V., and Zhaxybayeva, O. (2021). Evolution of DNA packaging in gene transfer agents. Virus Evol. *7*, veab015.

Farrera-Calderon, R.G., Pallegar, P., Westbye, A.B., Wiesmann, C., Lang, A.S., and Beatty, J.T. (2021). The CckA-ChpT-CtrA phosphorelay controlling *Rhodobacter capsulatus* Gene Transfer Agent production is bidirectional and regulated by Ccclic di-GMP. J. Bacteriol. *203*.

Feklístov, A., Sharon, B.D., Darst, S.A., and Gross, C.A. (2014). Bacterial sigma factors: a historical, structural, and genomic perspective. Annu. Rev. Microbiol. *68*, 357–376.

Fogg, P.C.M. (2019). Identification and characterization of a direct activator of a gene transfer agent. Nat. Commun. *10*, 595.

Fogg, M.J., and Wilkinson, A.J. (2008). Higher-throughput approaches to crystallization and crystal structure determination. Biochem. Soc. Trans. *36*, 771–775.

Fogg, P.C.M., Westbye, A.B., and Beatty, J.T. (2012). One for all or all for one: heterogeneous expression and host cell lysis are key to gene transfer agent activity in *Rhodobacter capsulatus*. PLoS ONE *7*, e43772.

Freese, H.M., Sikorski, J., Bunk, B., Scheuner, C., Meier-Kolthoff, J.P., Spröer, C., Gram, L., and Overmann, J. (2017). Trajectories and drivers of genome evolution in surface-associated marine *Phaeobacter*. Genome Biol. Evol. *9*, 3297–3311.

Fujikawa, N., Kurumizaka, H., Nureki, O., Terada, T., Shirouzu, M., Katayama, T., and Yokoyama, S. (2003). Structural basis of replication origin recognition by the DnaA protein. Nucleic Acids Res. *31*, 2077–2086.

Gabler, F., Nam, S.-Z., Till, S., Mirdita, M., Steinegger, M., Söding, J., Lupas, A.N., and Alva, V. (2020). Protein sequence analysis using the MPI bioinformatics toolkit. Curr. Protoc. Bioinformatics *72*, e108.

Geertz, M., Travers, A., Mehandziska, S., Sobetzko, P., Chandra-Janga, S., Shimamoto, N., and Muskhelishvili, G. (2011). Structural coupling between RNA polymerase composition and DNA supercoiling in coordinating transcription: a global role for the omega subunit? MBio *2*.

Glyde, R., Ye, F., Jovanovic, M., Kotta-Loizou, I., Buck, M., and Zhang, X. (2018). Structures of bacterial RNA polymerase complexes reveal the mechanism of DNA loading and transcription initiation. Mol. Cell *70*, 1111-1120.e3.

Goddard, T.D., Huang, C.C., Meng, E.C., Pettersen, E.F., Couch, G.S., Morris, J.H., and Ferrin, T.E. (2018). UCSF ChimeraX: Meeting modern challenges in visualization and analysis. Protein Sci. *27*, 14–25.

Griffith, K.L., Shah, I.M., Myers, T.E., O'Neill, M.C., and Wolf, R.E. (2002). Evidence for "pre-recruitment" as a new mechanism of transcription activation in *Escherichia coli*: the large excess of SoxS binding sites per cell relative to the number of SoxS molecules per cell. Biochem. Biophys. Res. Commun. *291*, 979–986.

Gunnelius, L., Hakkila, K., Kurkela, J., Wada, H., Tyystjärvi, E., and Tyystjärvi, T. (2014). The omega subunit of the RNA polymerase core directs transcription efficiency in cyanobacteria. Nucleic Acids Res. *42*, 4606–4614.

He, Y. (2012). Analyses of *Brucella* pathogenesis, host immunity, and vaccine targets using systems biology and bioinformatics. Front. Cell. Infect. Microbiol. *2*, 2.

Hynes, A.P., Mercer, R.G., Watton, D.E., Buckley, C.B., and Lang, A.S. (2012). DNA packaging bias and differential expression of gene transfer agent genes within a population during production and release of the *Rhodobacter capsulatus* gene transfer agent, RcGTA. Mol. Microbiol. *85*, 314–325.

Hynes, A.P., Shakya, M., Mercer, R.G., Grüll, M.P., Bown, L., Davidson, F., Steffen, E., Matchem, H., Peach, M.E., Berger, T., *et al.* (2016). Functional and evolutionary characterization of a gene transfer agent's multilocus "genome". Mol. Biol. Evol. *33*, 2530–2543.

Jumper, J., Evans, R., Pritzel, A., Green, T., Figurnov, M., Ronneberger, O., Tunyasuvunakool, K., Bates, R., Žídek, A., Potapenko, A., *et al.* (2021). Highly accurate protein structure prediction with AlphaFold. Nature *596*, 583–589.

Kaczmarczyk, A., Vorholt, J.A., and Francez-Charlot, A. (2013). Cumate-inducible gene expression system for sphingomonads and other Alphaproteobacteria. Appl. Environ. Microbiol. *79*, 6795–6802.

Karimova, G., Pidoux, J., Ullmann, A., and Ladant, D. (1998). A bacterial two-hybrid system based on a reconstituted signal transduction pathway. Proc Natl Acad Sci USA *95*, 5752–5756.

Kogay, R., Neely, T.B., Birnbaum, D.P., Hankel, C.R., Shakya, M., and Zhaxybayeva, O. (2019). Machine-learning classification suggests that many alphaproteobacterial prophages may instead be Gene Transfer Agents. Genome Biol. Evol. *11*, 2941–2953.

Kogay, R., Wolf, Y.I., Koonin, E.V., and Zhaxybayeva, O. (2020). Selection for reducing energy cost of protein production drives the GC content and amino acid composition bias in gene transfer agents. MBio *11*, e01206-20.

Koppenhöfer, S., Wang, H., Scharfe, M., Kaever, V., Wagner-Döbler, I., and Tomasch, J. (2019). Integrated transcriptional regulatory network of quorum sensing, replication control, and SOS response in *Dinoroseobacter shibae*. Front. Microbiol. *10*, 803.

Kuchinski, K.S., Brimacombe, C.A., Westbye, A.B., Ding, H., and Beatty, J.T. (2016). The SOS response master regulator LexA regulates the Gene Transfer Agent of *Rhodobacter capsulatus* and represses transcription of the signal transduction protein CckA. J. Bacteriol. *198*, 1137–1148.

Kurkela, J., Fredman, J., Salminen, T.A., and Tyystjärvi, T. (2021). Revealing secrets of the enigmatic omega subunit of bacterial RNA polymerase. Mol. Microbiol. *115*, 1–11.

Lane, W.J., and Darst, S.A. (2006). The structural basis for promoter -35 element recognition by the group IV sigma factors. PLoS Biol. *4*, e269.

Lang, A.S., and Beatty, J.T. (2000). Genetic analysis of a bacterial genetic exchange element: the gene transfer agent of *Rhodobacter capsulatus*. Proc Natl Acad Sci USA *97*, 859–864.

Lang, A.S., Zhaxybayeva, O., and Beatty, J.T. (2012). Gene transfer agents: phage-like elements of genetic exchange. Nat. Rev. Microbiol. *10*, 472–482.

Leung, M., and Beatty, J. (2013). *Rhodobacter capsulatus* Gene Transfer Agent transduction assay. Bio Protoc *3*.

Leung, M.M., Brimacombe, C.A., Spiegelman, G.B., and Beatty, J.T. (2012). The GtaR protein negatively regulates transcription of the *gtaRI* operon and modulates gene transfer agent (RcGTA) expression in *Rhodobacter capsulatus*. Mol. Microbiol. *83*, 759–774.

Lin, W., Mandal, S., Degen, D., Cho, M.S., Feng, Y., Das, K., and Ebright, R.H. (2019). Structural basis of ECF-σ-factor-dependent transcription initiation. Nat. Commun. *10*, 710.

Livak, K.J., and Schmittgen, T.D. (2001). Analysis of relative gene expression data using real-time quantitative PCR and the 2(-Delta Delta C(T)) Method. Methods *25*, 402–408.

Li, L., Fang, C., Zhuang, N., Wang, T., and Zhang, Y. (2019). Structural basis for transcription initiation by bacterial ECF σ factors. Nat. Commun. *10*, 1153.

Maniatis, T., Fritsch, E.F., and Sambrook, J. (1982). Molecular cloning: A laboratory manual. Cold Spring Harbor laboratory press.

Mao, C., Zhu, Y., Lu, P., Feng, L., Chen, S., and Hu, Y. (2018). Association of ω with the C-Terminal region of the β' Subunit Is essential for assembly of RNA polymerase in *Mycobacterium tuberculosis*. J. Bacteriol. *200*.

966 Martin, R.G., Gillette, W.K., Martin, N.I., and Rosner, J.L. (2002). Complex formation
967 between activator and RNA polymerase as the basis for transcriptional activation by
968 MarA and SoxS in *Escherichia coli*. Mol. Microbiol. *43*, 355–370.

969 Mathew, R., and Chatterji, D. (2006). The evolving story of the omega subunit of
970 bacterial RNA polymerase. Trends Microbiol. *14*, 450–455.

971 McDaniel, L.D., Young, E., Delaney, J., Ruhnau, F., Ritchie, K.B., and Paul, J.H. (2010).
972 High frequency of horizontal gene transfer in the oceans. Science *330*, 50.

973 Mercer, R.G., Callister, S.J., Lipton, M.S., Pasa-Tolic, L., Strnad, H., Paces, V., Beatty,
974 J.T., and Lang, A.S. (2010). Loss of the response regulator CtrA causes pleiotropic
975 effects on gene expression but does not affect growth phase regulation in *Rhodobacter*
976 *capsulatus*. J. Bacteriol. *192*, 2701–2710.

977 Mercer, R.G., Quinlan, M., Rose, A.R., Noll, S., Beatty, J.T., and Lang, A.S. (2012).
978 Regulatory systems controlling motility and gene transfer agent production and release
979 in *Rhodobacter capsulatus*. FEMS Microbiol. Lett. *331*, 53–62.

980 Motro, Y., La, T., Bellgard, M.I., Dunn, D.S., Phillips, N.D., and Hampson, D.J. (2009).
981 Identification of genes associated with prophage-like gene transfer agents in the
982 pathogenic intestinal spirochaetes *Brachyspira hyodysenteriae*, *Brachyspira pilosicoli*
983 and *Brachyspira intermedia*. Vet. Microbiol. *134*, 340–345.

984 Narasimhan, G., Bu, C., Gao, Y., Wang, X., Xu, N., and Mathee, K. (2002). Mining
985 protein sequences for motifs. J. Comput. Biol. *9*, 707–720.

986 Paget, M.S. (2015). Bacterial sigma factors and anti-sigma factors: structure, function
987 and distribution. Biomolecules *5*, 1245–1265.

988 Pallegar, P., Peña-Castillo, L., Langille, E., Gomelsky, M., and Lang, A.S. (2020a).
989 Cyclic di-GMP-mediated regulation of gene transfer and motility in *Rhodobacter*
990 *capsulatus*. J. Bacteriol. *202*.

991 Pallegar, P., Canuti, M., Langille, E., Peña-Castillo, L., and Lang, A.S. (2020b). A two-
992 component system acquired by horizontal gene transfer modulates gene transfer and
993 motility via cyclic dimeric GMP. J. Mol. Biol. *432*, 4840–4855.

994 Price, M.N., Wetmore, K.M., Waters, R.J., Callaghan, M., Ray, J., Liu, H., Kuehl, J.V.,
995 Melnyk, R.A., Lamson, J.S., Suh, Y., *et al.* (2018). Mutant phenotypes for thousands of
996 bacterial genes of unknown function. Nature *557*, 503–509.

997 Québatte, M., and Dehio, C. (2019). *Bartonella* gene transfer agent: Evolution, function,
998 and proposed role in host adaptation. Cell. Microbiol. *21*, e13068.

Québatte, M., Christen, M., Harms, A., Körner, J., Christen, B., and Dehio, C. (2017). Gene Transfer Agent promotes evolvability within the fittest subpopulation of a bacterial pathogen. Cell Syst. *4*, 611-621.e6.

Ross, W., Vrentas, C.E., Sanchez-Vazquez, P., Gaal, T., and Gourse, R.L. (2013). The magic spot: a ppGpp binding site on *E. coli* RNA polymerase responsible for regulation of transcription initiation. Mol. Cell *50*, 420–429.

Salmon-Divon, M., Zahavi, T., and Kornspan, D. (2019). Transcriptomic analysis of the *Brucella melitensis* Rev.1 vaccine strain in an acidic environment: Insights Into virulence attenuation. Front. Microbiol. *10*, 250.

Schindelin, J., Arganda-Carreras, I., Frise, E., Kaynig, V., Longair, M., Pietzsch, T., Preibisch, S., Rueden, C., Saalfeld, S., Schmid, B., *et al.* (2012). Fiji: an open-source platform for biological-image analysis. Nat. Methods *9*, 676–682.

Scholz, H.C., Pfeffer, M., Witte, A., Neubauer, H., Al Dahouk, S., Wernery, U., and Tomaso, H. (2008). Specific detection and differentiation of *Ochrobactrum anthropi*, *Ochrobactrum intermedium* and *Brucella* spp. by a multi-primer PCR that targets the recA gene. J. Med. Microbiol. *57*, 64–71.

Shakya, M., Soucy, S.M., and Zhaxybayeva, O. (2017). Insights into origin and evolution of α-proteobacterial gene transfer agents. Virus Evol. *3*, vex036.

Sherlock, D., Leong, J.X., and Fogg, P.C.M. (2019). Identification of the first gene transfer agent (GTA) small terminase in *Rhodobacter capsulatus*, its role in GTA production and packaging of DNA. J. Virol. *93*, e01328-19.

Shimada, T., Yamazaki, Y., Tanaka, K., and Ishihama, A. (2014). The whole set of constitutive promoters recognized by RNA polymerase RpoD holoenzyme of *Escherichia coli*. PLoS ONE *9*, e90447.

Sievers, F., Wilm, A., Dineen, D., Gibson, T.J., Karplus, K., Li, W., Lopez, R., McWilliam, H., Remmert, M., Söding, J., *et al.* (2011). Fast, scalable generation of high-quality protein multiple sequence alignments using Clustal Omega. Mol. Syst. Biol. *7*, 539.

Solovyev, V., A Salamov (2011) Automatic annotation of microbial genomes and metagenomic equences. In Metagenomics and its Applications in Agriculture, Biomedicine and Environmental Studies (Ed. R.W. Li), Nova Science Publishers, p.61-78.

Tamarit, D., Neuvonen, M.-M., Engel, P., Guy, L., and Andersson, S.G.E. (2018). Origin and evolution of the *Bartonella* gene transfer agent. Mol. Biol. Evol. *35*, 451–464.

Tomasch, J., Wang, H., Hall, A.T.K., Patzelt, D., Preusse, M., Petersen, J., Brinkmann, H., Bunk, B., Bhuju, S., Jarek, M., *et al.* (2018). Packaging of *Dinoroseobacter shibae* DNA into Gene Transfer Agent particles is not random. Genome Biol. Evol. *10*, 359–369.

Vassylyev, D.G., Sekine, S., Laptenko, O., Lee, J., Vassylyeva, M.N., Borukhov, S., and Yokoyama, S. (2002). Crystal structure of a bacterial RNA polymerase holoenzyme at 2.6 A resolution. Nature *417*, 712–719.

Wall, J.D., Weaver, P.F., and Gest, H. (1975). Gene transfer agents, bacteriophages, and bacteriocins of *Rhodopseudomonas capsulata*. Arch. Microbiol. *105*, 217–224.

Wang, H., Ziesche, L., Frank, O., Michael, V., Martin, M., Petersen, J., Schulz, S., Wagner-Döbler, I., and Tomasch, J. (2014). The CtrA phosphorelay integrates differentiation and communication in the marine alphaproteobacterium *Dinoroseobacter shibae*. BMC Genomics *15*, 130.

Waterhouse, A.M., Procter, J.B., Martin, D.M.A., Clamp, M., and Barton, G.J. (2009). Jalview Version 2--a multiple sequence alignment editor and analysis workbench. Bioinformatics *25*, 1189–1191.

Weiss, A., Moore, B.D., Tremblay, M.H.J., Chaput, D., Kremer, A., and Shaw, L.N. (2017). The ω subunit governs RNA polymerase stability and transcriptional specificity in *Staphylococcus aureus*. J. Bacteriol. *199*.

Westbye, A.B., Leung, M.M., Florizone, S.M., Taylor, T.A., Johnson, J.A., Fogg, P.C., and Beatty, J.T. (2013). Phosphate concentration and the putative sensor kinase protein CckA modulate cell lysis and release of the *Rhodobacter capsulatus* gene transfer agent. J. Bacteriol. *195*, 5025–5040.

Westbye, A.B., O'Neill, Z., Schellenberg-Beaver, T., and Beatty, J.T. (2017). The *Rhodobacter capsulatus* gene transfer agent is induced by nutrient depletion and the RNAP omega subunit. Microbiology *163*, 1355–1363.

Westbye, A.B., Kater, L., Wiesmann, C., Ding, H., Yip, C.K., and Beatty, J.T. (2018). The protease ClpXP and the PAS domain protein DivL regulate CtrA and Gene Transfer Agent production in *Rhodobacter capsulatus*. Appl. Environ. Microbiol. *84*.

Wiethaus, J., Wirsing, A., Narberhaus, F., and Masepohl, B. (2006). Overlapping and specialized functions of the molybdenum-dependent regulators MopA and MopB in *Rhodobacter capsulatus*. J. Bacteriol. *188*, 8441–8451.

Wiethaus, J., Schubert, B., Pfänder, Y., Narberhaus, F., and Masepohl, B. (2008). The GntR-like regulator TauR activates expression of taurine utilization genes in *Rhodobacter capsulatus*. J. Bacteriol. *190*, 487–493.

1068 Yamamoto, K., Yamanaka, Y., Shimada, T., Sarkar, P., Yoshida, M., Bhardwaj, N.,
1069 Watanabe, H., Taira, Y., Chatterji, D., and Ishihama, A. (2018). Altered distribution of
1070 RNA polymerase lacking the Omega subunit within the prophages along the
1071 *Escherichia coli* K-12 genome. MSystems *3*.

1072 Zimmermann, L., Stephens, A., Nam, S.-Z., Rau, D., Kübler, J., Lozajic, M., Gabler, F.,
1073 Söding, J., Lupas, A.N., and Alva, V. (2018). A completely reimplemented MPI
1074 bioinformatics toolkit with a new HHpred server at its core. J. Mol. Biol. *430*, 2237–2243.

Figure 1

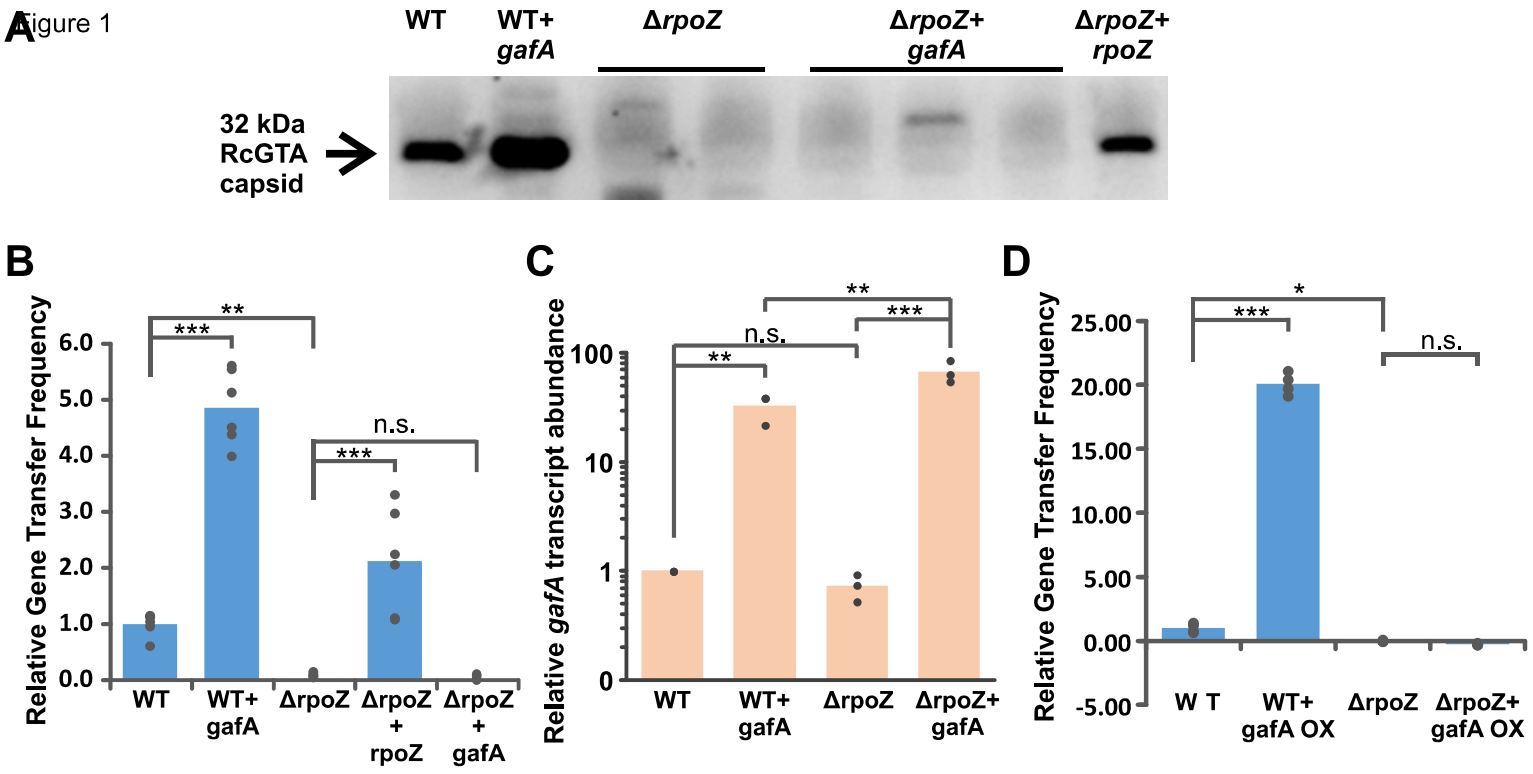
A
WT
WT+ gafA
ΔrpoZ
ΔrpoZ+ gafA
ΔrpoZ+ rpoZ
32 kDa RcGTA capsid
B
Relative Gene Transfer Frequency
6.0
5.0
4.0
3.0
2.0
1.0
0.0
**
***
n.s.
***
WT
WT+ gafA
ΔrpoZ
ΔrpoZ + rpoZ
ΔrpoZ + gafA
C
Relative gafA transcript abundance
100
10
1
0
**
n.s.
**
***
WT
WT+ gafA
ΔrpoZ
ΔrpoZ+ gafA
D
Relative Gene Transfer Frequency
25.00
20.00
15.00
10.00
5.00
0.00
-5.00
*
***
n.s.
W T
WT+ gafA OX
ΔrpoZ
ΔrpoZ+ gafA OX

Figure 2

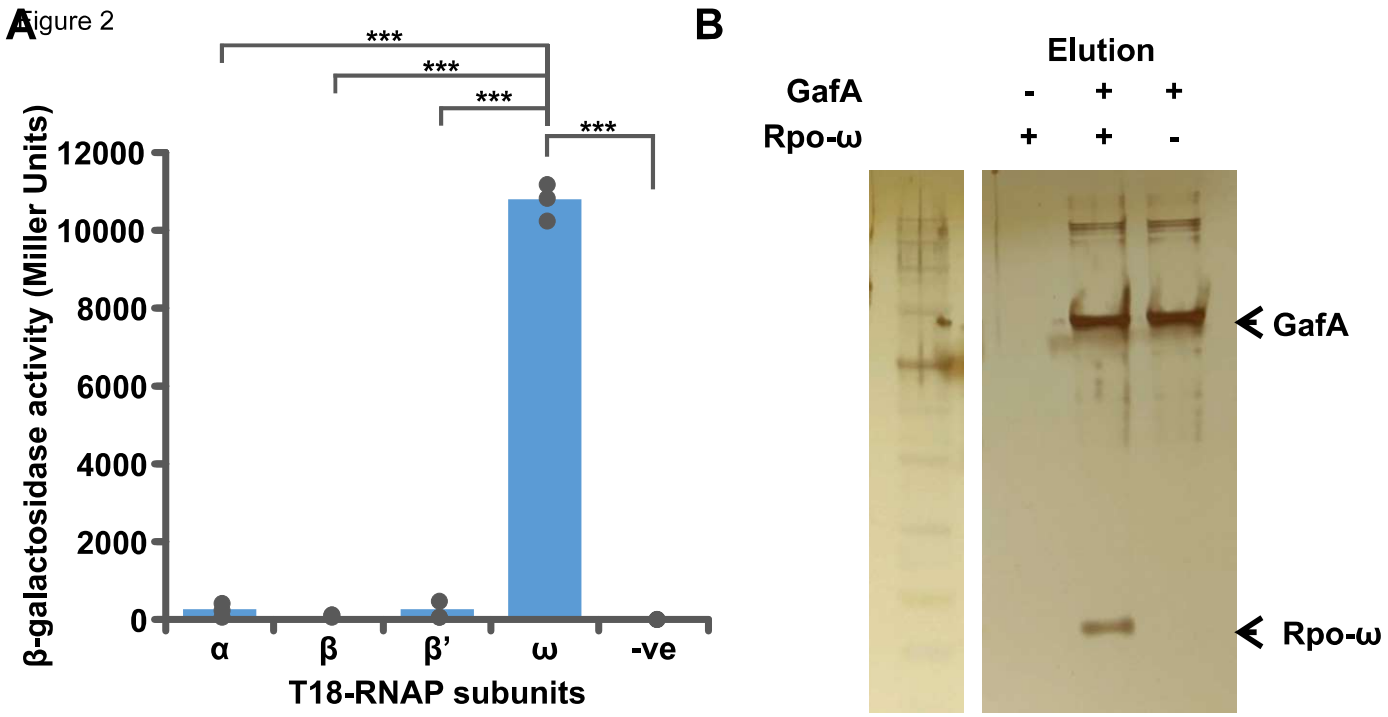
A
***
***
***
***
12000
10000
8000
6000
4000
2000
0
β-galactosidase activity (Miller Units)
α
β
β'
ω
-ve
T18-RNAP subunits
B
Elution
GafA - + +
Rpo-ω + + -
GafA
Rpo-ω

Figure 3

A

>GafA_1-382

MKTMQDRESLPDWLPDHARLYLRHVEEGVPIRQLARAEG
CHASTILRRVRRIEQRRDDPLVDEALTRLGRFAAAASAA
PPREDDPAMTAPIRPTAPQACPEAAEDPDSPDIATLSRE
GRRVLRRLAEPGALLIIAPDMEKAVVLRGTVRTAVVARE
VAQGFALNGWILVQHSGRVTSYELSATGRAALKRLLEAE
ALTAGRDPATAADNPHADRHRDWGERTVNEGQGRVTRMR
MNLAESPLGVLARRRDSDGRPFLSPDLVAAGERLREDFE
LAQMGPRVAQNWERFMTGGARGQYRPELGHGGPGGSDRA
RERVAAALCDLGPGLGDMVLRCCCFLEGLETAEKRMGWS
ARSGKIVLRIALMRLKRHYDETYGGAAPLIG

B

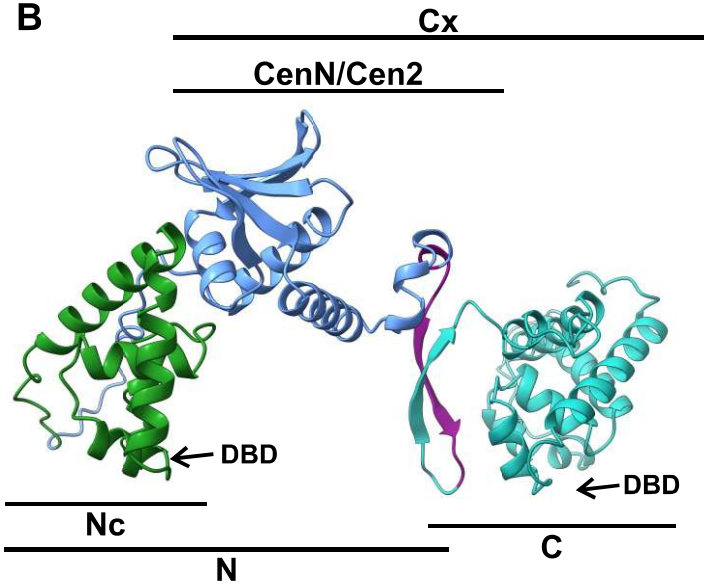

C

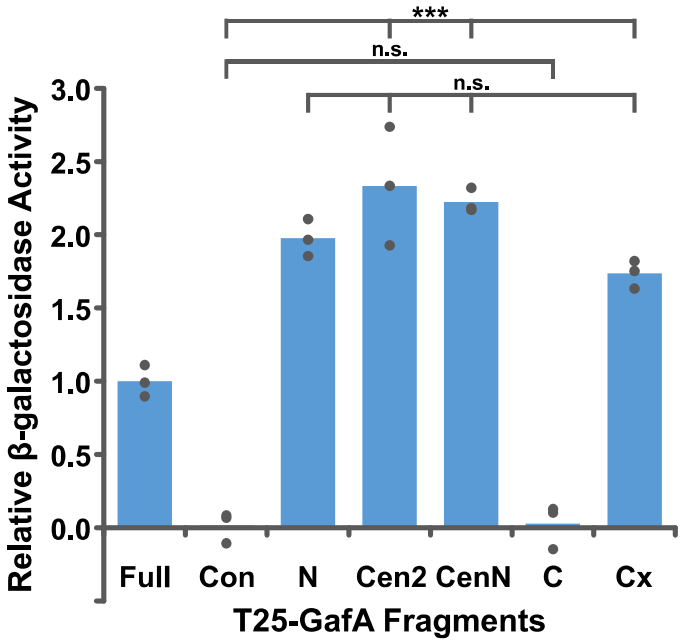

D

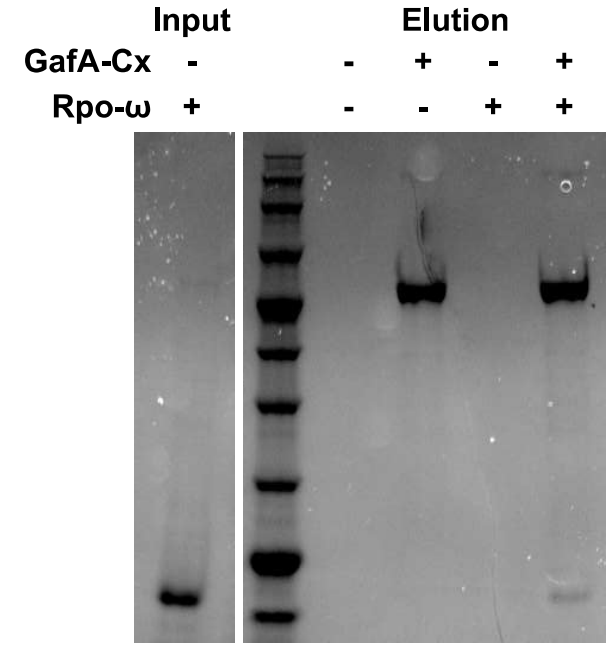

Figure 4

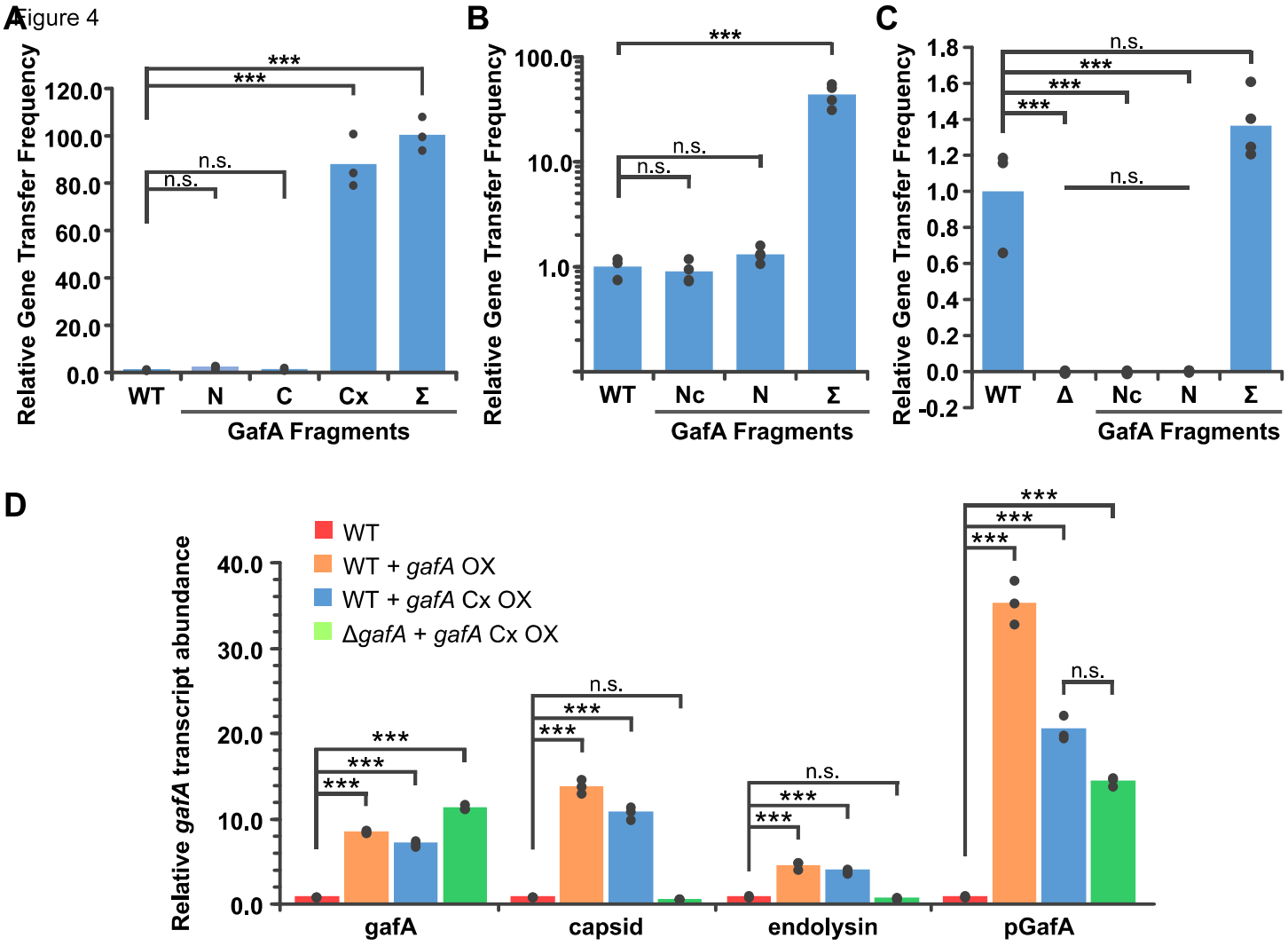
A
Relative Gene Transfer Frequency
120.0
100.0
80.0
60.0
40.0
20.0
0.0
***
***
n.s.
n.s.
WT
N
C
Cx
Σ
GafA Fragments
B
Relative Gene Transfer Frequency
100.0
10.0
1.0
***
n.s.
n.s.
WT
Nc
N
Σ
GafA Fragments
C
Relative Gene Transfer Frequency
1.8
1.6
1.4
1.2
1.0
0.8
0.6
0.4
0.2
0.0
-0.2
n.s.
***
***
***
n.s.
WT
Δ
Nc
N
Σ
GafA Fragments
D
Relative gafA transcript abundance
40.0
30.0
20.0
10.0
0.0
WT
WT + gafA OX
WT + gafA Cx OX
ΔgafA + gafA Cx OX
***
***
***
n.s.
***
***
n.s.
***
***
***
***
***
n.s.
gafA
capsid
endolysin
pGafA

Figure 5

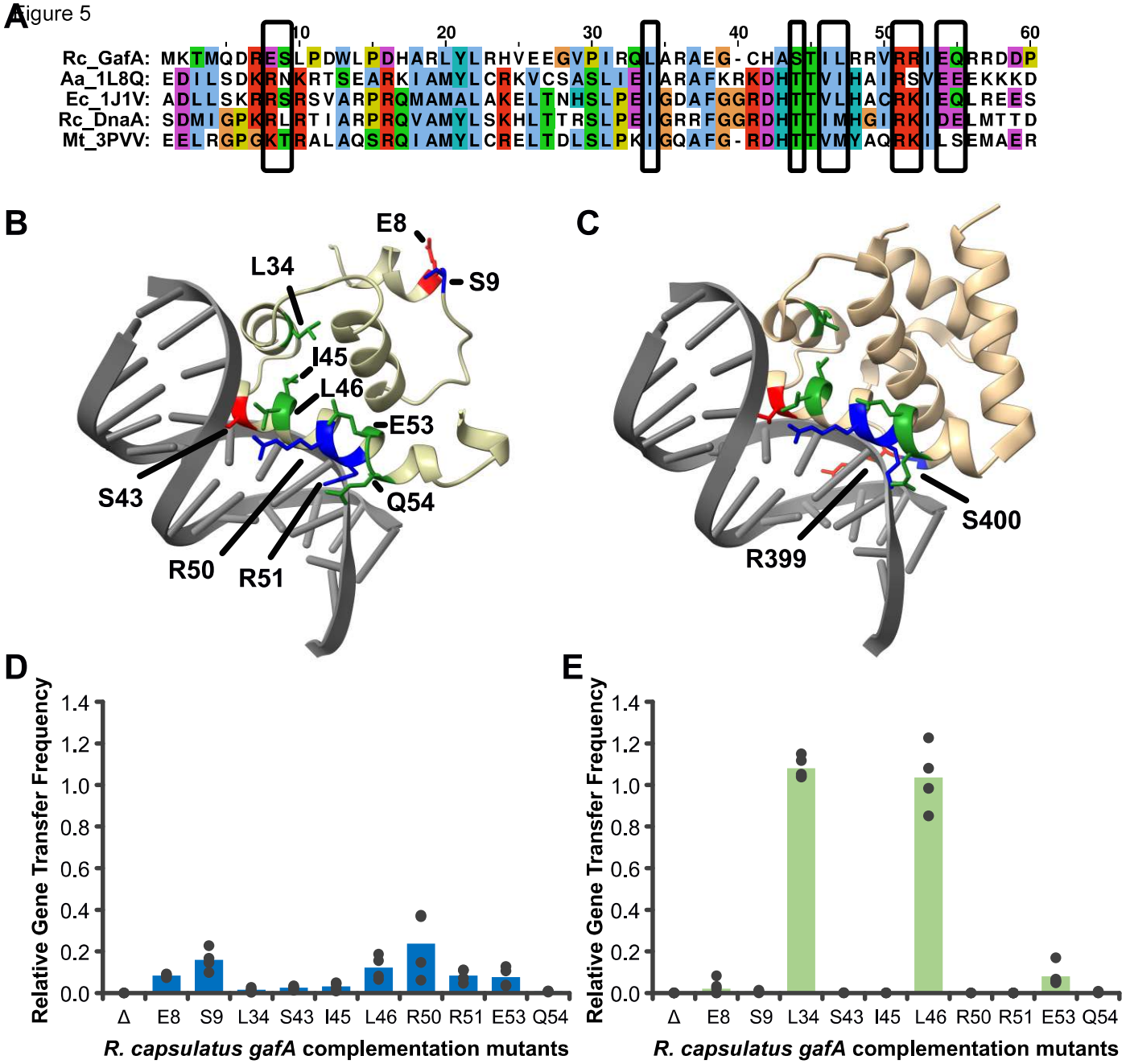
A
10
20
30
40
50
60
Rc_GafA: MKTMQDRESLPDWLPDHARLYLRHVEEGVPIRQLARAEG-CHASTILRRVRRIEQRRDDP
Aa_1L8Q: EDILSDKRNKRTSEARKIAMYLCRKVCSASLIEIARAFKRKDHTTVIHAIRSVEEEKKKD
Ec_1J1V: ADLLSKRRSRSVARPRQMAMALAKELTNHSLPEIGDAFGGRDHTTVLHACRKIEQLREES
Rc_DnaA: SDMIGPKRLRTIARPRQVAMYLSKHLTTRSLPEIGRRFGGRDHTTIMHGIRKIDELMTTD
Mt_3PVV: EELRGPGKTRALAQSRQIAMYLCRELTDLSLPKIGQAFG-RDHTTVMYAQRKILSEMAER
B
E8
S9
L34
I45
L46
E53
S43
Q54
R50
R51
C
S400
R399
D
Relative Gene Transfer Frequency
1.4
1.2
1.0
0.8
0.6
0.4
0.2
0.0
Δ E8 S9 L34 S43 I45 L46 R50 R51 E53 Q54
R. capsulatus gafA complementation mutants
E
Relative Gene Transfer Frequency
1.4
1.2
1.0
0.8
0.6
0.4
0.2
0.0
Δ E8 S9 L34 S43 I45 L46 R50 R51 E53 Q54
R. capsulatus gafA complementation mutants

Figure 6

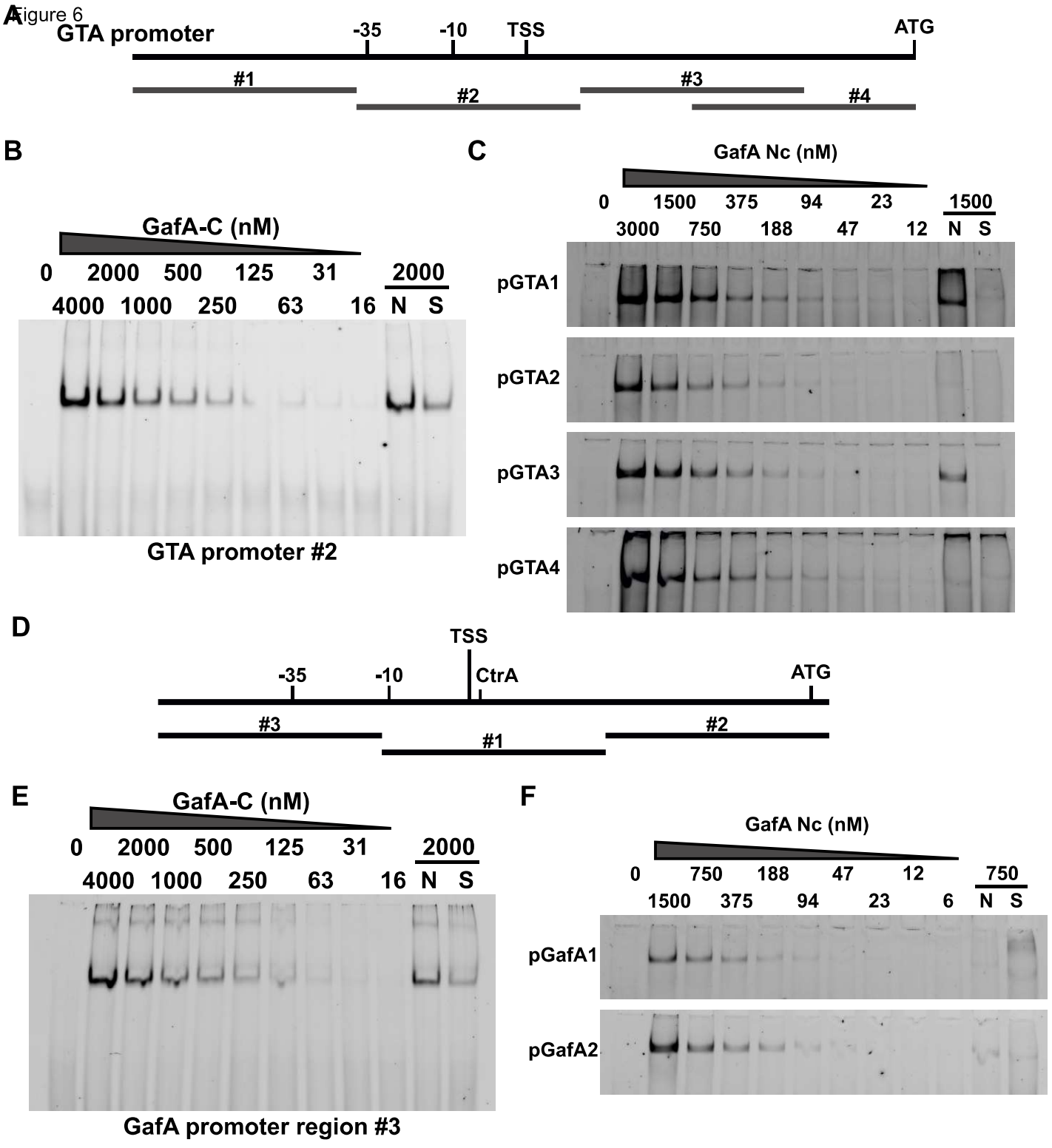
A
GTA promoter
-35
-10
TSS
ATG
#1
#2
#3
#4
B
GafA-C (nM)
0 2000 500 125 31
2000
4000 1000 250 63 16 N S
GTA promoter #2
C
GafA Nc (nM)
0 1500 375 94 23
1500
3000 750 188 47 12 N S
pGTA1
pGTA2
pGTA3
pGTA4
D
TSS
-35
-10
CtrA
ATG
#3
#1
#2
E
GafA-C (nM)
0 2000 500 125 31
2000
4000 1000 250 63 16 N S
GafA promoter region #3
F
GafA Nc (nM)
0 750 188 47 12
750
1500 375 94 23 6 N S
pGafA1
pGafA2

Figure 7

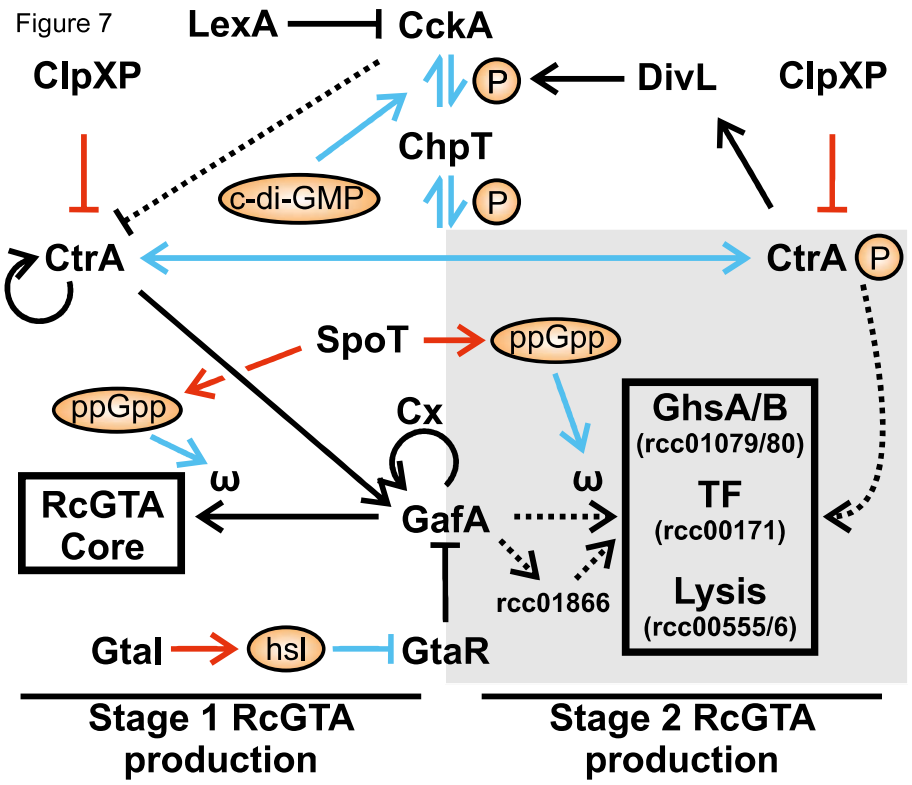
LexA
CckA
ClpXP
P
DivL
ClpXP
ChpT
c-di-GMP
P
CtrA
CtrA
P
SpoT
ppGpp
ppGpp
Cx
GhsA/B
(rcc01079/80)
TF
(rcc00171)
Lysis
(rcc00555/6)
ω
ω
RcGTA
Core
GafA
rcc01866
GtaI
hsl
GtaR
Stage 1 RcGTA
production
Stage 2 RcGTA
production

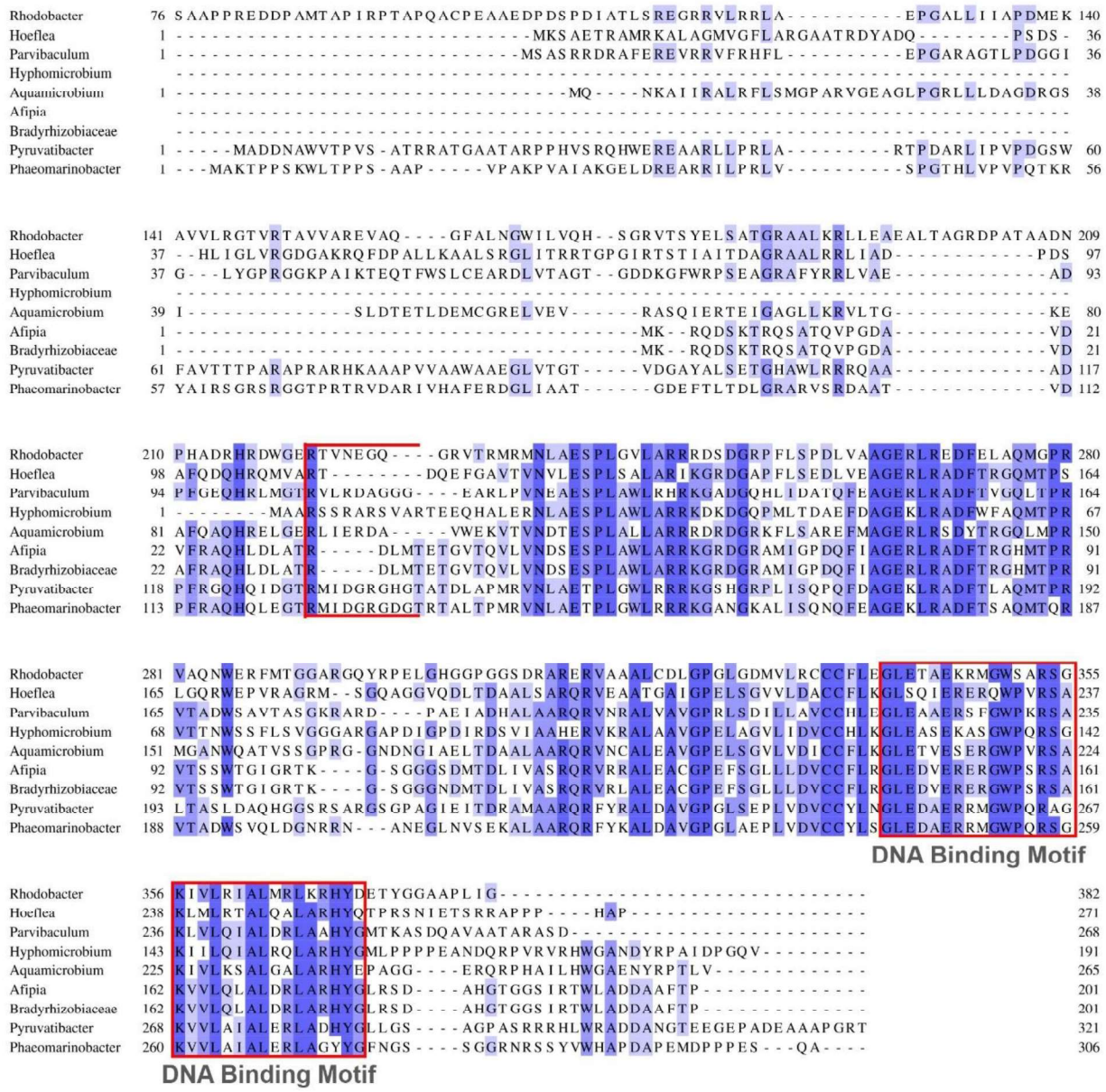

Figure S1. Alignment of the *R. capsulatus* GafA C-terminal extended domain with Hyphomicrobiales counterparts. Related to Figure 3. The top four hits against fully assembled Hyphomicrobiales genomes were chosen from separate BLASTp and PSI-BLAST sequence similarity searches with an *R. capsulatus* GafA query. Conservation is indicated with the Jalview percentage identity colour scheme. The predicted C-terminal DNA binding domain is boxed and annotated to highlight increased sequence conservation. The open box indicated the beginning of the C-terminal concise constructs.

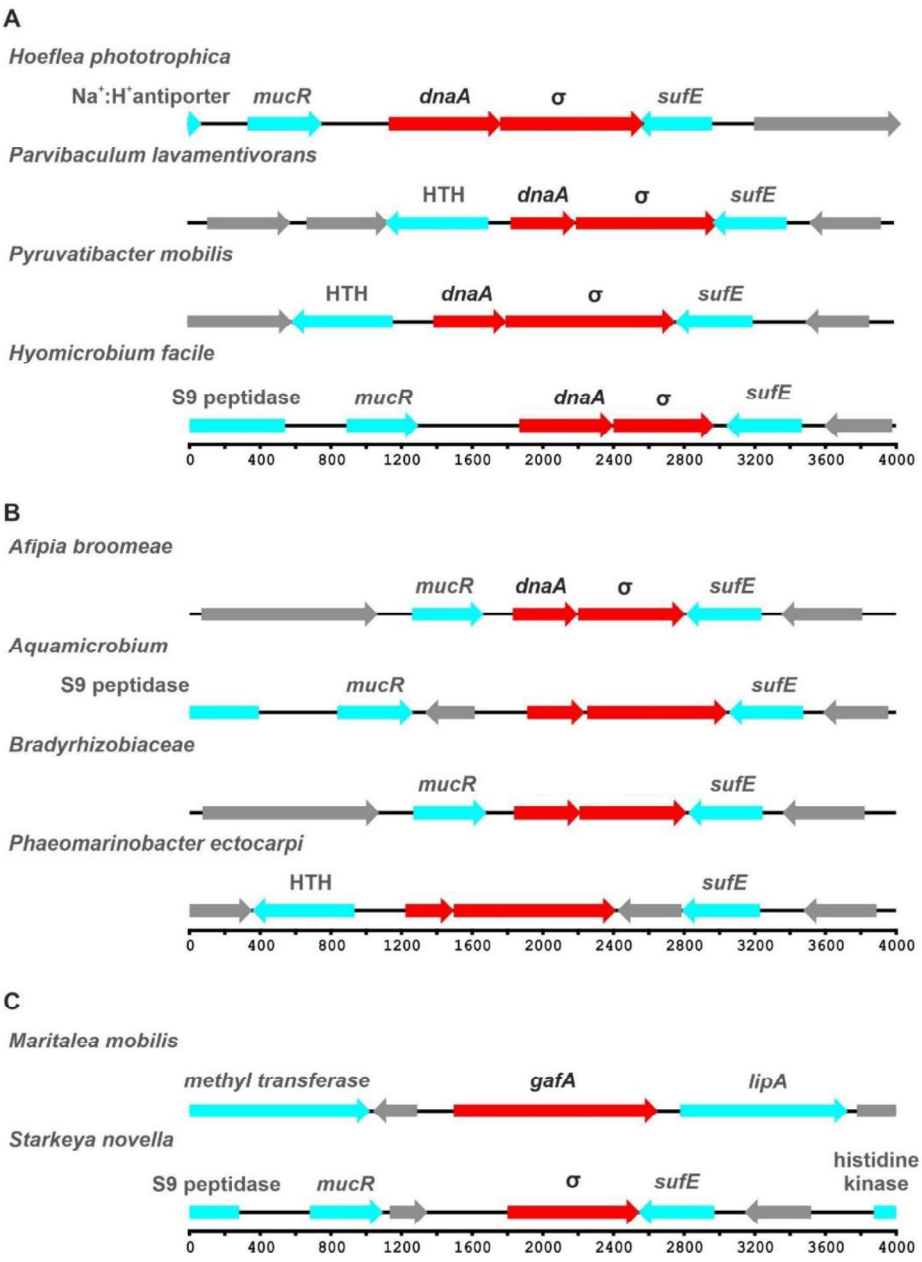

Figure S2. Synteny plots for Hyphomicrobiales GafA homologues. Related to Figure 3. The top four **A.** BLASTp and **B.** PSI-BLAST hits for *R. capsulatus* GafA against fully assembled Hyphomicrobiales genomes. Sequence matches mainly occurred for the GafA C-terminal region only with genes annotated as DUF6456 domain-containing proteins. The matched Hyphomicrobiales genes are annotated here using the HHPRED prediction of a Sigma factor-like domain (σ) and the ORF is coloured red. The upstream dnaA-like ORF is also coloured red. Flanking genes with predicted function are cyan, hypothetical proteins of unknown function are grey. **C.** Two exceptions are shown where either a full-length match was obtained but with Rhodoabcterales-like synteny (*Maritalea*) or the *dnaA* gene was absent with otherwise Hyphomicrobiale-like synteny (*Starkeya*). Scale bars are provided below each panel in bases.

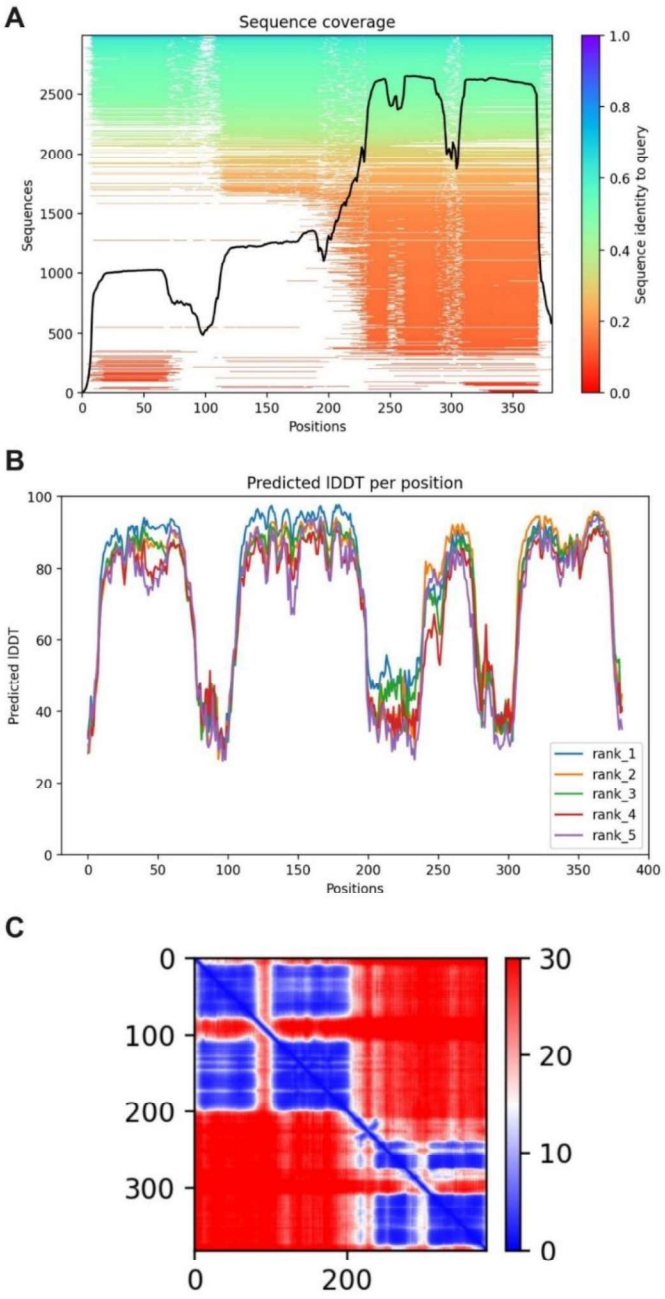

Figure S3. Confidence outputs for *R. capsulatus* GafA structure prediction. Related to Figure 3. A. The jackhmmer method was used on the Alphafold server to align GafA to related proteins and the multiple sequence alignment coverage plot is shown. Aligned sequence coverage is depicted as a line chart and sequence identity is colour coded as shown in the legend. **B.** AlphaFold output plot showing the predicted local Distance Difference Test score (pIDDT) confidence metric. Amino acid positions are shown on the X-axis. **C.** Predicted Aligned Error for each amino acid position labelled on the X and Y-axes. Error is shown on a scale of 0-30, and colour coded as shown in the legend. Clear drop-offs in model confidence can be seen between predicted domains, but each domain is has strong scores typically >80.

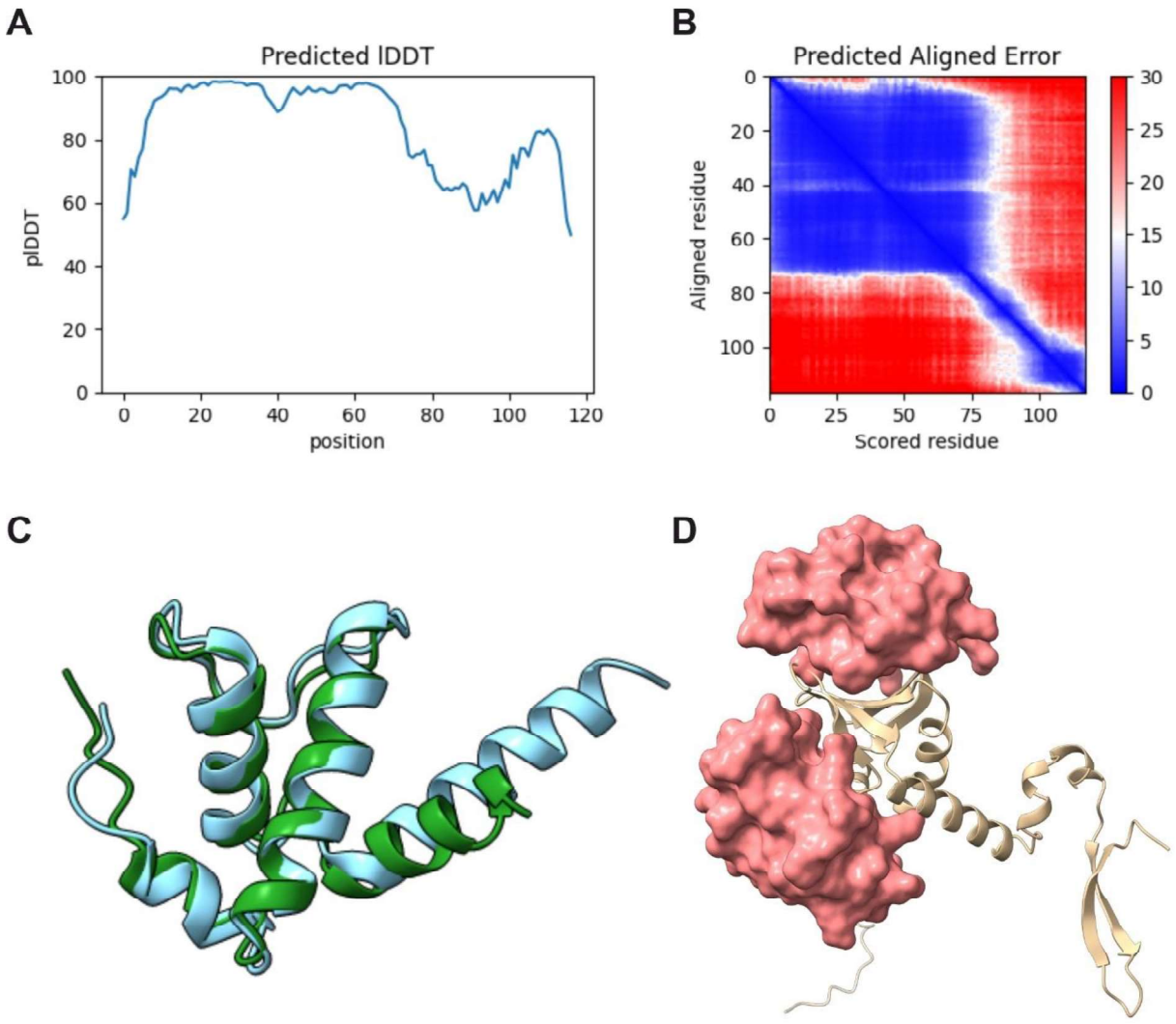

Figure S4. Predicted structure of *R. capsulatus* Rpo-ω protein and its interaction with GafA. Related to Figure 3. A & B. AlphaFold output plots showing the predicted local Distance Difference Test score (pIDDT) confidence metric and Predicted Aligned Error for each amino acid position. A clear drop-off in model confidence, domain packing and broader topology is observed from approximately residue 70 onwards. **C.** AlphaFold predicted *R. capsulatus* Rpo-ω structure trimmed to residues 1-71 (green) and overlaid with *E. coli* Rpo-ω, PDB: 6ALF (pale blue). **D.** LZerD protein docking predictions for GafA-CenN and Rpo-ω^{1-71}. The two Rpo-ω surface structures shown are representatives of the two centroid clusters that comprise the top ten interaction models. The upper location in contact with the β-sheet was favoured by 6 out of 10 models including the top ranked (rank sum = 47).

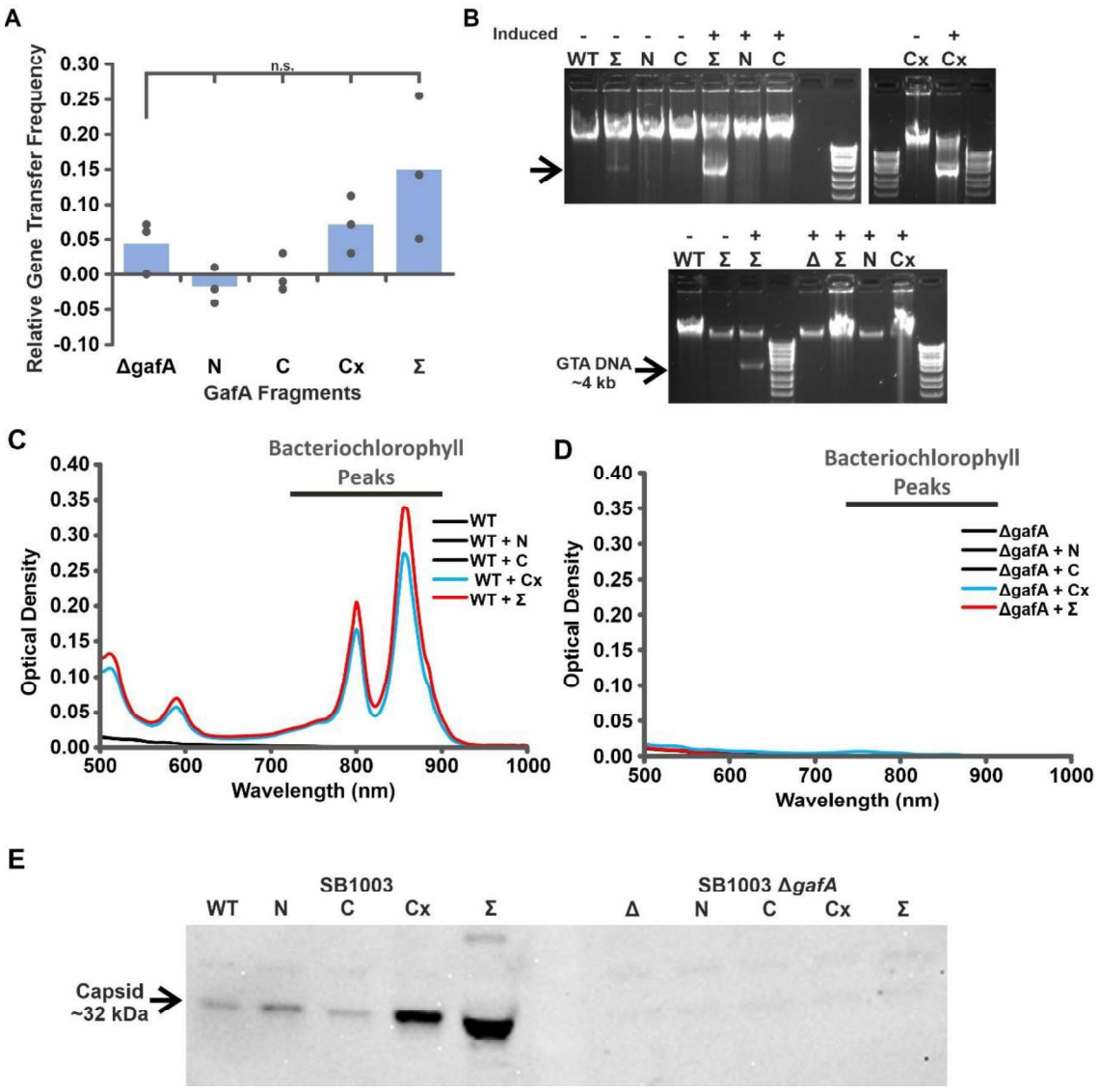

Figure S5. RcGTA production phenotypes after *in trans* expression of GafA full length and truncated proteins. Related to Figure 4. In all panels, SB1003 wild-type and a Δ*gafA* derivative were complemented with empty pQF vector (WT or Δ) or pQF containing truncated *gafA* genes as indicated (*gafA*-N, *gafA*-C, *gafA*-Cx, *gafA*-Σ). **A.** Chart of the frequency of rifampicin gene transfer from *R. capsulatus* SB1003 Δ*gafA* donor strains complemented *in trans* with the indicated pQF vectors, N = 3. **B.** Total intracellular DNA content showing the presence or absence of characteristic 4 kb RcGTA DNA. **C.** Mean absorbance trace of *R. capsulatus* SB1003 supernatant or **D.** SB1003 Δ*gafA* supernatants in the 500-1000 nm wavelength range. Complementation *in trans* the pQF plasmid containing full-length *gafA* is represented by a red line, with *gafA-Cx* is represented by a cyan line and all other constructs (pQF-empty, *gafA*-N and *gafA*-C) are shown in black. N=6 except Δ*gafA* + Cx N=4. Distinctive bacteriochlorophyll peaks indicating cells lysis are annotated. **E.** Representative western blot of concentrated supernatant from the indicated *R. capsulatus* strains using an α-RcGTA capsid antibody. See also Data S1.

A

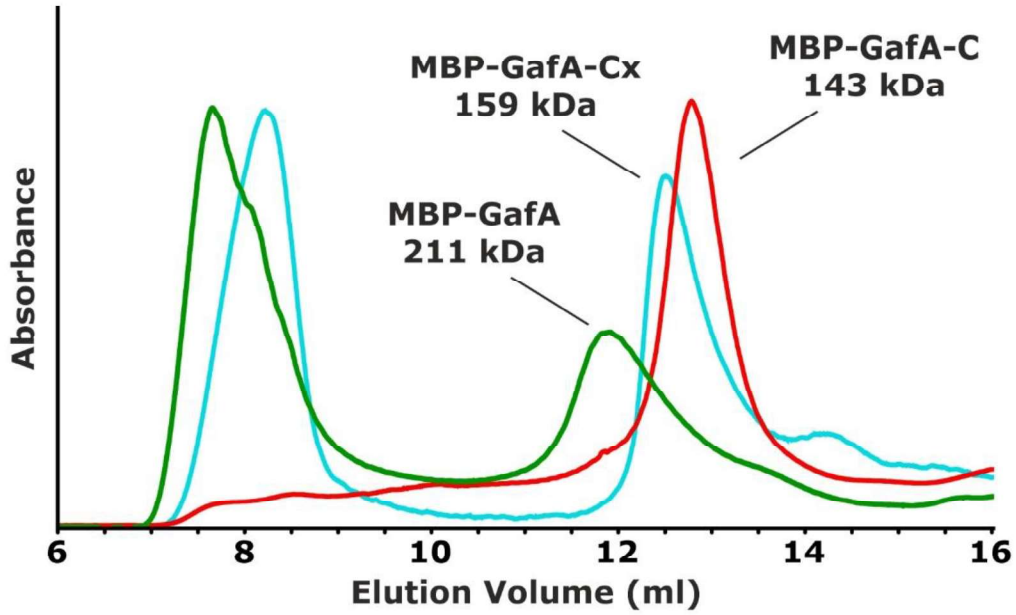

B

Protein	Elution Peak (ml)	Estimated MW (kDa)	Monomer Size (kDa)	Ratio
MBP-GafA-Cx	12.54	158,779	75,806	2.1
MBP-GafA-C	12.78	142,537	61,119	2.3
MBP-GafA	11.91	210,774	85,159	2.5

Figure S6. Analytical gel filtration of GafA proteins. Related to Figure 6. A. Representative traces showing absorbance of GafA (green), GafA-Cx (cyan) and GafA-C (red) at 280 nm versus elution time from the column. Absorbance values are omitted on the Y-axis because the traces are scaled differently to improve comparability. **B.** Summary table of values plotted in part A, the estimated MW of the protein peaks, the calculated MW of each monomer and the ratio of observed MW to that of the monomer.

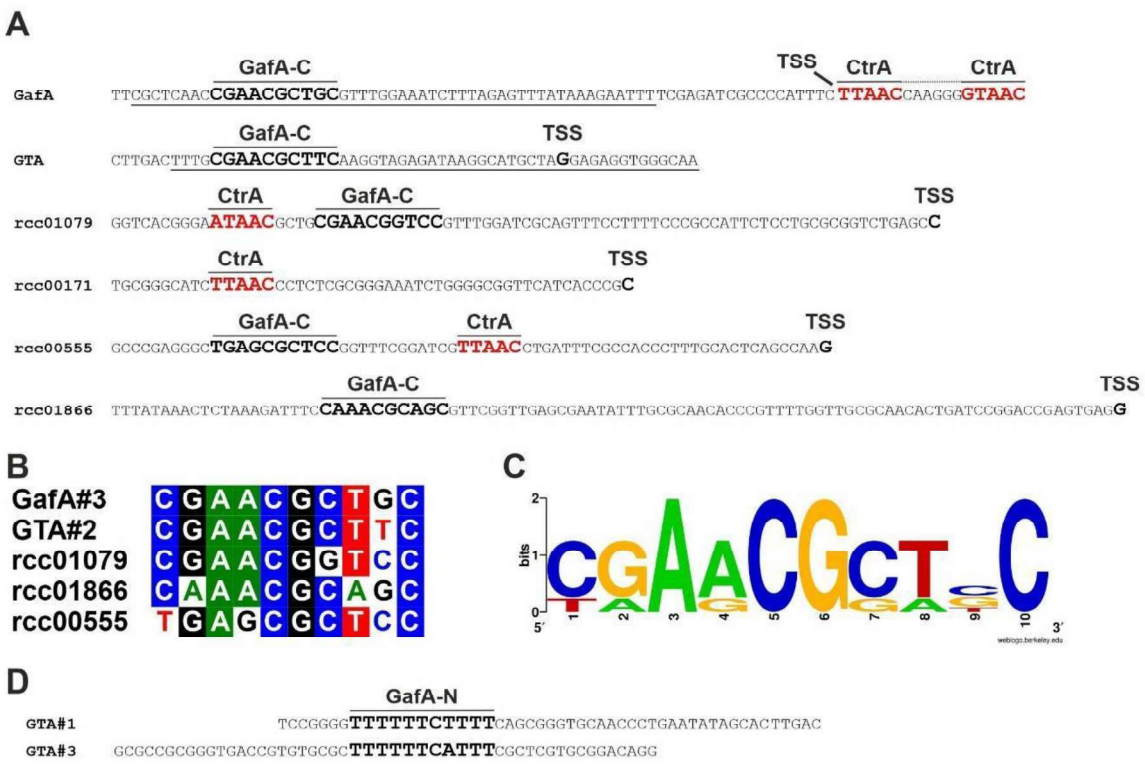

Figure S7. Predicted binding sites for GafA N/C-terminal DNA binding domains. Related to Figure 6. **A.** Schematic of RcGTA related promoters. Transcription start sites (TSS) were estimated based on published RNAseq data. Predicted CtrA binding sites/half-sites are highlighted in bold red and annotated, predicted GafA C-terminal (GafA-C) DNA binding sites are highlighted in bold black and annotated. Underlined sequence indicates the region used for EMSA band shift assays. The five predicted GafA-C binding sites are depicted in **B.** an alignment and **C.** a Logo plot. **D.** The two oligo sequences that were specifically bound by the GafA N-terminal DNA binding domain (GafA-N) are shown with the putative binding site aligned, emboldened and annotated.